Textural insights into the significance of ophiolitic chromitites, with special reference to Oman

Françoise Boudier, David Mainprice, Adolphe Nicolas, Fabrice Barou

▶ **To cite this version:**

Françoise Boudier, David Mainprice, Adolphe Nicolas, Fabrice Barou. Textural insights into the significance of ophiolitic chromitites, with special reference to Oman. Tectonophysics, 2021, 814, ⟨10.1016/j.tecto.2021.228972⟩. ⟨insu-03661289⟩

HAL Id: insu-03661289

https://insu.hal.science/insu-03661289v1

Submitted on 2 Aug 2023

HAL is a multi-disciplinary open access archive for the deposit and dissemination of scientific research documents, whether they are published or not. The documents may come from teaching and research institutions in France or abroad, or from public or private research centers.

L'archive ouverte pluridisciplinaire **HAL**, est destinée au dépôt et à la diffusion de documents scientifiques de niveau recherche, publiés ou non, émanant des établissements d'enseignement et de recherche français ou étrangers, des laboratoires publics ou privés.

Distributed under a Creative Commons CC BY-NC 4.0 - Attribution - Non-commercial use - International License

Version of Record: https://www.sciencedirect.com/science/article/pii/S0040195121002547
Manuscript_0ec49cefb3c2cd3e22388194f67139a8

Textural insights into the significance of ophiolitic chromitites, with special reference to Oman.

Françoise Boudier, David Mainprice, Adolphe Nicolas and Fabrice Barou,

Geosciences Montpellier, CNRS & Université de Montpellier 2, F-34095 Montpellier, France

Corresponding author: Françoise Boudier, Université de Montpellier 2, 34095 Montpellier,

e-mail : francoise.boudier@umontpellier.fr

Keywords: Chromite crystallization; Semail ophiolite; upper mantle dynamics; crystal preferred orientation; misorientation at grain boundary; melt circulation.

ABSTRACT

This paper analyses the process and depth of formation of chromite crystals occasionally including ultrahigh pressure (UHP) minerals, recovered from some investigated ophiolites. We present direct microstructural evidence for crystallization of chromite ores from the Semail ophiolite, in place they are exposed. Similar crystal preferred orientation in olivine-rich layers and in septa from chromite layers indicate deformation of the olivine solid frame by dislocation creep at high temperature, synchronous with the crystallization of chromite. The preservation of the olivine framework throughout the development of joined chromite grains suggests that chromite replaced olivine. Chromite grains crystallized from a melt circulating in an open-system, stress-bearing network of dunitic aggregate, controlled by the olivine high-T slip system. The misorientation of joined crystals at grain boundaries define the ratio of twin vs. random boundaries that were closed to vs. open to fluid circulation, respectively, suggesting that chromite layers may represent planes of channelized melt circulation. The relationship of chromite deposits to ridge tectonics structures suggests that Cr-bearing melt was produced at the transition from an active spreading ridge to deep mantle shear zones acting as possible source of hydration. The occurrence of

© 2021 published by Elsevier. This manuscript is made available under the CC BY NC user license
https://creativecommons.org/licenses/by-nc/4.0/

potential UHP inclusions in chromite crystals is assigned to continental contamination of melts ascending through the Arabian margin.

1. Introduction

The distribution of chromitite deposits in ophiolites is highly uncertain; some ophiolites contain exceptionally large reserves estimated over a million tons, whereas others do not contain chromitite (Boudier & Al Rajhi, 2014). Most chromitite deposits are lying at the Moho transition zone (MTZ), or occasionally in the uppermost harzburgitic section, and are always included in a dunitic envelope (Nicolas, 1989). Around 200 chromitite deposits have been reported in Oman by various groups (Augé, 1987; Augé and Roberts, 1982; Ceuleneer and Nicolas, 1985; Christiansen, 1985; Nicolas and Al Azri, 1991; Michel, 1993). Ore deposits are relatively small, under 10,000 tons, and only a few pods exceed 30,000 tons.

Previous studies of the Oman ophiolite (Augé, 1987; Arai, 1994; Arai et al., 2006) have distinguished Cr-rich chromites in Wadi Rajmi from Al-rich chromites in the Maqsad MTZ. Ahmed and Arai (2002) point to a link between high PGE concentration and high Cr# in chromites located at depth in the mantle section of Hilti Massif. Rollinson (2008), Rollinson et al. (2012), provided detailed geochemical data on the different Oman chromites, pointing to a difference in the calculated melt in equilibrium with Cr-rich chromites vs Al-rich chromites. The first are highly magnesian primitive 'arc type' melt, the second evolving toward mid ocean ridge basalt. Structurally, Boudier and Al Rajhi (2014) related the distribution of pods to the internal structure of the ophiolite.

Recently, the identification of ultrahigh-pressure (UHP) microphases included in some chromite aggregates from ophiolites of Tethyan paleo-sutures (Robinson et al., 2004) and from the Polar Ural (Savelieva et al., 2007) have provided important constraints on chromitite genesis. These UHP phases comprise zircon, titanite, corundum, kyanite, coesite, metal alloy, diamond and moissanite, some being found in situ, hosted in chromite and olivine crystals from the chromitite deposits (Yang, 2015). Moissanite has been identified in Cr-rich chromitite from Shamis II deposit of Wadi Rajmi (Trumble et al., 2009). These occurrences are highly enigmatic, calling for a

continental contamination in the system of genesis of chromitite deposits (Robinson et al., 2015; Trumbull et al., 2009).

These results call into question the timing and location of the formation of chromite crystals encapsulating UHP phases in podiform chromitite deposits from some ophiolites, which, if known, would make chromite a powerful indicator of the former tectonic setting of mafic-ultramafic rocks. Here, referring to Semail ophiolite occurrences, we tentatively trace the timing and location of chromite crystallization through the textural relationship between chromite grains and their hosting dunite.

2. Semail chromitites, structural approach

Based on detailed field studies in New Caledonia, the structural classification of chromitite deposits proposed by Cassard et al. (1981), stresses the relationship of variable geometry of chromitite pods and the mantle flow fabrics in their enclosing peridotite (inset, Fig. 1). These relationships apply to ophiolitic chromitite ores exposed in the Semail ophiolite and provide first-order data on their formation.

At the scale of a given ophiolite like Semail, chromitite deposits of the order of ten thousand tons do not occur regularly along the paleo-ridge axis (Fig. 1). In the southern district, parts of the pods are located in the thick MTZ topping mantle diapirs, like the large domain of Maqsad (Jousselin et al., 1998). Others, particularly in the northern district, are located underneath the Moho transition zone, at the margin of kilometers wide shear zones (Boudier and Al-Rajhi, 2014).

Four chromitite deposits, representative for their textural type, were selected for this study (Fig. 1). Both discordant “dike” and concordant “stratiform” belong to the thick MTZ of Maqsad mantle diapir in the southern Sumail massif. The second discordant deposit is also located at MTZ of the southern Sumail massif, along Wadi Sahara. Only the concordant layered deposit belongs to the northern domain, the chromite-rich district of Wadi Rajmi.

2. 1. The Maqsad area

The Maqsad area (Fig. 2a) exposes a thick (up to 300 m) MTZ atop a mantle diapir recognized by steep lineation (high-T mantle flow lines) recorded in the harzburgitic

section. These directions rotate abruptly to a flat diverging trend (corner flow) at the MTZ (Jousselin et al., 1998). The diapir is assumed to represent punctuation on a ridge axis of regional NNW-SSE trend (Nicolas et al., 2000). The exposed MTZ includes a relatively large number of chromitite deposits of moderate size and various types. The Maqsad zone extends over ~10 km and, to the west, abuts on a mega-shear zone identified at the regional scale, punctuated by granitic intrusions (Rabu et al., 1986).

The concordant stratiform chromitite deposit (90OA62), northwest of Tuff area (Fig. 2a), is located ~5 km north from the center of the Maqsad mantle diapir, in the median part of the ~170m thick MTZ, a level where dry dunite evolves to an interlayering of dunite, wehrlite and olivine-bearing gabbro at centimetric to metric scale (Boudier and Nicolas, 1995; Higgie and Tommasi, 2012). This "Tuf stratiform" chromitite deposit exposes massive chromite layers a few meters thick (Fig. 3a), interlayered with tens of meters thick layers of disseminated chromitite and dunite, all parallel to the gently southwest-dipping regional foliation.

The discordant chromite pod ("dike" 83OG58) is located on the ridge east of Tuf garden in the Maqsad area (Fig. 2a), at the very top of the MTZ, just beneath the layered gabbro section. The pod has the geometry of a vertical cavity (Fig. 3b) devoid of any plastic deformation, providing the opportunity to observe pristine magmatic textures. The ore is composed of a spectacular nodular texture, largely studied since its initial discovery (Ceuleneer and Nicolas, 1985 ; Lorand and Ceuleneer, 1989 ; Leblanc and Ceuleneer, 1992). Chromite nodules are flattened parallel to a rough dunite/ chromitite layering.

2. 2. The Sahara zone

The Sahara zone, located in the northwest part of exposed mantle in Sumail massif (Fig. 1), represents a linear feeding zone trending parallel to the inferred ridge axis in this massif (Nicolas et al., 2000). High-T lineations rotate from the direction of spreading to axis-parallel and the regional flat foliation steepens parallel to the ridge axis. The feeding zone is also marked by a ridge-parallel diabase dike swarm, cutting through the lithosphere.

The "Sahara" chromitite occurrence (93OF13) consists of three main ore bodies of the discordant type (inset, Fig. 1) included in a 1 km x 200 m dunite zone, under extension (Fig. 3c). The discordant bodies are dominantly composed of massive dunite

interlayered with ''antinodular'' chromitite aggregates. The internal structure is marked in the three bodies by folds having the steep foliation as axial plane, and fold axis at high angle to the flat mineral lineation (B-folds). The southward plunging structures suggest a continuation below the wadi level. The chromitite is of massive to antinodular type, often banded.

2. 3. The Wadi Rajmi

The Wadi Rajhmi represents the richest district of chromite production in Oman. Chromite deposits are distributed either at Mohio level or, among the largest ores, near the Wadi Rajmi major shear zone (Fig 2b). The Wadi Rajmi shear zone is one of the several NW-SE trending shear zones, that cross-cut the mantle section in Fizh and North-Hilti massifs, and are nearly parallel to the sheeted dike trend (Fig. 1). In these kilometer-wide shear zones, swarms of numerous pyroxenite and gabbro dikes are highly stretched and boudined, indicative of a sustained magma supply during continuing deformation.

The "Shamis II" chromitite in Wadi Rajmi area is located in the harzburgitic mantle (Fig. 2b), within one kilometer from the major shear zone (Boudier and Al-Rajhi, 2014). Shamis II (Fig. 3d) is a large, discontinuous chromitite nappe ~10 m thick and ~100 m in extension, and comprising massive and disseminated chromitite layers. The chromitite nappe and its dunitic envelope are slightly discordant on the enclosing harzburgite foliation. The area is crosscut by numerous pyroxenite and gabbro dikes, trending at high angle to the mineral lineation.

3. Textures and Crystallographic Orientation Data

3. 1. Sampling and methods.

To further characterize the relationship of chromite crystals with their dunite enclosure, we have analyzed the crystal-preferred orientation (CPO) of chromite crystals and their enclosing olivine aggregates. Due to the poor visibility of the spinel shape fabric (the strain marker) in the dunite at the sample scale, thin section were cut perpendicular to the chromitite layering (Fig. 4), instead of the finite strain reference

stem (foliation and lineation) as is usual for kinematic studies (Nicolas, 1989). For this reason, the CPO pole figures reported herein are not referenced to the principal X and Z strain axes, somewhat limiting the identification of the olivine acting slip system.

The CPOs of olivine and chromite were acquired via indexation of electron back-scattered diffraction (EBSD) patterns. EBSD measurements were performed on a JEOL JSM5600 scanning electron microscope coupled to a CamScan X500FE Crystal Probe equipped with a HKL Nordlys camera, and using the HKL Channel 5 suite of programs, installed at Géosciences Montpellier. Textural analysis was performed using MTEX, an open-source MATLAB toolbox for textural analysis (https://mtex-toolbox.github.iol/, Bachmann et al., 2010).

For each sample we obtained a crystallographic orientation map covering a representative part (30 and 60%) of the thin section (Fig. 4). Data are presented as one measurement per pixel. The indexation reference phases are Fo_{100} (forsterite) for olivine and $MgCr_{2O4}$ for chromite. Average raw indexation rates are around 77%. EBSD mapping provides information on the distribution of both mineral phases olivine and chromite (phase map), crystal preferred orientation (CPO) for each phase (orientation map), detailed relationships at grain boundaries, and visualizes misorientation at sub-boundaries. Pole figures are represented using Euler angles with one datapoint per pixel. Maximum and minimum densities are expressed in times of uniform distribution.

3. 2. Nodular texture 83OG58.

This spectacular texture, represented in a dike-type discordant deposit, is composed of regular orbicular centimeters-sized chromite aggregates, flattened in a layering plane, and within a homogeneous, moderately serpentinized olivine matrix (Fig. 4a). The EBSD phase map (Fig. 5a) shows that chlorite and lizardite are concentrated in the center of chromite nodules and along crosscutting microcracks. Chlorite is also associated with lizardite in the hydrous network invading olivine. A few spots of pargasitic amphibole are present in olivine and as micrometer scale inclusions in chromite. The EBSD orientation map and pole figures (Fig. 5b and c) reveals chromite nodules composed of millimetric equigranular grains, devoid of crystallographic preferred orientation, limited by curviplanar grain boundaries. The enclosing olivine exhibits a continuous crystallographic orientation, indicating that the olivine matrix is composed of centimeters-sized undeformed crystals, signing their magmatic origin.

198 The EBSD orientation pattern corroborates the crystallization model proposed
199 earlier by Ceuleneer and Nicolas (1985) and Leblanc and Ceuleneer (1992), which
200 proposes chromite crystals growth in an open system supplied by Cr-rich melt.
201 Convective cells in a confined part of the sub-vertical conduit led to the aggregation of
202 fractionated chromite crystals into centimetric nodules segregated at the base of the
203 layers, and flattened. The residual fractionated melt was then frozen as olivine aggregate
204 preserved from further deformation.
205
206 **3. 3. Interstitial texture 90OA62**.
207 The interstitial texture is developed in a 'stratiform' deposit located at the base of a
208 gabbro lens, west of Tuf area, in the median part of the Maqsad MTZ. The chromite-rich
209 bands do not depart texturally from their olivine-rich margins. Optical observation (Fig.
210 4b and insert 1) point to localization of chromite crystals at grain-boundaries and sub-
211 boundaries of olivine porphyroclasts, Concave margins of irregular grain boundaries are
212 always oriented toward the olivine (Fig. 4b, insert 1), suggesting corrosion of olivine by
213 a growing chromite phase.
214 The olivine orientation map and pole figure (Fig. 6a) encompassing the chromite-
215 rich layer and olivine-rich margins confirms the residual character of the olivine grains,
216 which are marked by a strong planar fabric, controlled by the olivine slip plane (010). As
217 viewed in Figure 6a, the trace of the olivine slip plane (010) (the dashed white line), drawn
218 perpendicular to the [010] maximum, is at a low-angle to the compositional chromite layering
219 (the solid white line). Measured CPO of olivine is derived from all olivine grains in the
220 studied section, including olivine septa from the chromitite layer. The chromite
221 orientation map visualizes aggregates of chromite crystals 20-70 μm in size, limited by
222 planar boundaries, devoid of CPO as confirmed by the pole figure (Fig.6b).
223 Two important aspects of the interstitial texture are (1) the continuous transition
224 between olivine-rich and chromite-rich bands, which is only marked by the evolving
225 modal composition, and (2) the irregular olivine-chromite grain boundaries recording
226 corrosion of residual dunite by the growing chromite crystals. They lead to the
227 conclusion that chromite crystallized from a Cr-rich melt penetrating the anisotropic
228 porosity of the dunite matrix during or post high-T solid state flow.
229
230 **3. 4. Antinodular texture 93OF13.**

This texture observed in a series of discordant pods (Fig. 3c) is composed of fine-grained ''antinodules'' (50% olivine + 50% chromite) included in a chromitite matrix (85% chromite + 15% interstitial serpentinized olivine) (Fig. 4c). The ''antinodules'' have an oblate shape fabric, roughly parallel to the massive chromite layers (Fig. 4c).

The analysis of the olivine CPO (Fig. 7a) indicates that the olivine fraction in the ''antinodules'' is connected in 3D. All olivines exhibit a consistent strong orthorhombic CPO, with the (010) plane, the main slip plane in olivine, parallel to the flattening of the "antinodules". In addition, the olivine orientation map (Fig. 7a) marks a slight misorientation of subgrains within a given "antinodule". The chromite grains (Fig. 7b), 5-6µm sized in the chromitite matrix and 2µm in antinodules, are equigranular with planar grain-boundaries and devoid of CPO.

Interpretation of the antinodular texture must account for the fact that interstitial olivine exhibits a commmon high-T CPO, suggesting that the olivine aggregate was flowing during crystallization of chromite, and that the growing chromite network was passively deforming in the flowing olivine frame, leading to the antinodular network.

3. 5. Massive texture 84OA85.

This texture is representative of most massive chromitite deposits in the mining district of Rajmi. Massive chromitite bands containing 10% interstitial olivine are interlayered with dunite (Fig. 4d). The detailed optical image (Fig. 4d insert) visualizes a crystallographic continuity of olivine grains in the dunite with interstitial olivine septa in the chromitite, occasionally marked by subgrain boundaries. In addition, the imprint of high-T mantle flow in the dunite is clearly recorded by sharp subboundaries related with planar grain boundaries, attesting a high grade of restoration (Poirier and Nicolas, 1975). The EBSD olivine orientation map (Fig. 8a) confirms these characteristics. Pole figures measured in the dunite and chromitite band separately, exhibit an orthorhombic CPO in the dunite, with the olivine slip line [100] orthogonal to planar olivine grain boundaries. The interstitial olivine from chromitite exhibits a comparable CPO, although weaker. Chromite grains in the chromitite are equigranular, devoid of CPO, with jagged boundaries at contact of the interstitial olivine septa.

The high degree of restoration and strong orthorhombic olivine CPO in the dunite layer of this texture express the clear record of high-T asthenospheric mantle flow. The interesting point is the persistence of a comparable CPO in the interstitial deformed

olivine septa from the chromitite layer, leading to the conclusion that the chromite crystals accumulated in the residual dunite network after corrosion of the olivine by a Cr-rich melt having penetrated the anisotropic porosity of enclosing dunite.

4• Chromite/Olivine phase relationships: Grain boundary analysis

4. 1. Grain boundary analysis method.

We have applied to olivine-chromite relationships a method of grain boundary analysis developed in material sciences. Here we use our 2D EBSD data and the MTEX toolbox (https://mtex-toolbox.github.io, Mainprice et al., 2014). From the grain orientations (g. A) and (g. B) on either side of a boundary, we can calculate the misorientation at that boundary (Δg_AB = g_B . g_A-1). From the Δg AB matrix we can calculate the misorientation axis, and the misorientation angle about the axis. At each position along a boundary, MTEX calculates misorientations when grains of the same and different minerals are present on either side.

The objective in the studied case is to measure the misorientations along the grain boundaries (see section 4.2), paying special attention to boundaries that are twins. In chromite twin boundaries with special relationships (e.g. [111]/180°) are closed boundaries that will not allow fluids to flow along the boundary. Grain boundaries that have no special crystallographic relationships are identified as random boundaries, which are often open boundaries and allow fluids to flow (Shimada et al., 2002).

Searching for special relationship along olivine-olivine boundaries (i.e., the twin [100]/60°) returned only 4%, this is known to be a rare twin in olivine. We have also searched for the olivine to chromite relationship, such as parent (olivine) || child (chromite) which implies that chromite is the product of olivine, according to the topotactic relationship between the orthorhombic symmetry of olivine (forsterite) and the cubic symmetry of chromite (spinel): $(100)_{fo}$ || $(111)_{sp}$ and $[001]_{fo}$ || $[110]_{sp}$ (Fig. 9). Generally, twin boundaries and boundaries with topotactic relations are low energy boundaries that enhance corrosion resistance compared to other random boundaries of high energy which allow fluid percolation.

4. 2. Imaging of section 90OA62

We have applied this method to a large portion of the EBSD map of sample 90OA62 (Fig. 6). This section cut orthogonal to the chromite layering exposes olivine-rich layer, chromite-rich layer and a diopside-rich layer (Fig. 10a). We know from olivine CPO (fig. 6) that the dunite-chromite banding is at low angle to the $(010)_{ol}$ slip plane, sub-concordant to foliation.

As illustrated on figure 10a, we have detected the following types of grain boundaries: random olivine-olivine, random chromite-chromite, random olivine-chromite, twin chromite-chromite with [111] misorientation axis and angle 180°, twin olivine-olivine with [100] misorientation axis and angle 60°, and special topotactical olivine-chromite.

In the dunite band, large olivine grains contain chromite inclusions in a topotactic relationship (blue), and some olivine grains in twin relationship (light blue). Although present throughout the section, topotactic relations are rare and mostly restricted to the olivine-rich band. Chromite occurs mainly as finer grain size crystals along olivine boundaries or sub-boundaries.

The dense network of chromite in the chromite layer dominantly includes random chromite-chromite grain boundaries (black), with some twin boundaries (red). The predominance of random grain boundaries is corroborated by our analysis of the misorientation angles of correlated chromite grain boundaries (Fig. 10b). The misorientation angles distribution closely follows the theoretical red line, uniform or random distribution for cubic crystal symmetry, implying that chromite-chromite boundaries are dominantly random. The analysis of the rotation axes of misorientation angles below 10° is indicative of twinning, recorded by a maximum of the misorientation axis near [111] (Fig. 10c).

5• Discussion

5. 1. Textural record and kinematics of mantle flow

From the four studied samples representative of main chromite mining sites in Oman, two contrasted textural types are documented, based on the characteristics of the enclosing olivine aggregate (Fig. 11a). Type I, nodular is represented by a unique example of discordant dike. Type II, replaced texture, describe the three other textural

types, representative of variable mode and macroscopic distribution of chromite vs olivine.

5.1.1. The case of nodular texture. This texture is documented by a unique chromitite dike intrusive at top level of the MTZ in the Maqsad area. EBSD orientation patterns, revealing an undeformed aggregate of large centimetric olivine crystals enclosing nodular aggregates of millimetric idiomorphic chromite crystals (Fig. 5), have confirmed the model of chromite crystals nucleated from a mafic Cr-bearing melt, growing and aggregating in a dynamic mini-magma chamber atop the feeding dike (Ceuleneer and Nicolas, 1985; Lago et al., 1982; Nicolas, 1989; Leblanc and Ceuleneer, 1992).

5.1.2. Replaced textures. Similar chromite-olivine crystallographic relationships are documented in the three replaced textures (Figs. 6, 7, 8), representative of variable chromite/olivine ratio. These textures bear the print of high-T solid state flow in the enclosing olivine aggregate, marked by a high degree of restoration: straight boundaries and sharp sub-boundaries consistent with the deformation of olivine by dislocation creep at high-T (Nicolas and Poirier, 1976) particularly designed in the Shamis II sample 84OA85 (Fig. 4d). The three textures share a common olivine CPO pattern, marked by a clear concentration of the (010) slip plane. Both the [100] and [001] axes mark good maximum in samples 93OF13 and in the dunite from sample 84OA85, but their distribution gets more diffuse in the chromite-rich layers, particularly represented in sample 90OA62. As mentioned earlier, measured CPOs do not refer to the principal X and Z strain axes, due to the lack of strain markers in our samples, and the acting slip system is not totally defined. Nonetheless, the CPO of sample 90OA62 from Maqsad can be referred to previous study in peridotites from the same area (Boudier and Nicolas, 1995), which are marked by a strong maximum of the olivine (010) slip plane and [100] slip line slightly oblique to the strain markers foliation and lineation, thus interpreted in term of mantle flow in the asthenospheric conditions.

The same pattern describing the olivine-rich layers and the interstitial olivine septa from chromite-rich layers (Fig. 6, 7, 8), draws an olivine framework that is crystallographically continuous throughout the chromitite layering. This crystallographic continuity means that the olivine framework is residual, and that the joined olivine-chromite phases is not the product of olivine-chromite syncrystallization.

5.1.3. Chromite nucleation/growth and melt percolation. Our detailed analysis of grain boundaries in the Maqsad stratiform site 90OA62 (Fig.10) supports the view that the same crystallization process ruled the olivine-rich compared with chromite-rich bands: same idiomorphic millimetric chromite crystals, first distributed at olivine grain boundaries and sub-boundaries, then extending in the chromite-rich band (compositional layering). The preservation of the olivine framework throughout the development of joined chromite grains supports the replaced character of chromite to olivine. The increasing abundance of chromite-chromite boundaries dominantly random (Fig. 10a) would favor melt percolation and make the chromite-rich layers, channels of focused melt transfer, feeding olivine corrosion in a feedback stem. These channels produced the chromite layers, parallel to the dunite foliation, and controlled by the solid state flow of the olivine aggregate.

Interestingly a similar channelized fluid circulation has been inferred from a detailed textural-CPO study of a banded dunite/olivine gabbro in the Maqsad MTZ, in continuity with and located some hundreds of meters from the chromite site 90OA62 (Higgie and Tommasi, 2012). The strong olivine CPO is interpreted by the authors as resulting from deformation in the presence of melt circulating in an open stem, with instantaneous melt fraction below the critical threshold 20-40% allowing for the disruption of the solid stress-bearing network.

5. 2. Relationships with ridge tectonics

Based on the local structural mapping (Fig. 3), we stress that the solid state deformation documented in the chromite-enclosing dunite is consistent with both local mantle flow structures (foliation, lineation) and regional structures recorded in the main mantle section (Nicolas et al., 2000).

In a general compilation of chromite ore deposits in the Sultanate of Oman, Boudier and Al-Rajhi (2014) point to common relationships of chromite ore distribution with large lithospheric shear zones. This is best documented for the large mining district of Wadi Rajmi (Fig. 1 and 2b) where the main chromite ores are located in the harzburgitic section, below the MTZ. The Wadi Rajmi shear zone is one of several regional shear zones that structure the northern Oman ophiolitic massifs (Fig. 1). Trending at low angle to the paleo-spreading axis (Nicolas et al., 2000; Umino et al., 2003), these shear zones are relaying the high-T mantle flow under ductile conditions,

as shown by the progressive rotation of flow lines when steepening the flow plane (Boudier et al., 1988; Michibayashi et al., 2006) and by multiple injections of mafic melts coeval with shear zone activity. Not only at Wadi Rajmi, these shear zones are the sites of chromitite occurrences (Ahmed and Arai, 2002; Nicolas and Al-Azri, 1991; Boudier and Al Rajhi, 2014).

Focusing on the most documented Maqsad area, the other mining district, populated by numerous relatively small ore deposits (Fig. 2a), the largely exposed mantle diapir punctuating the assumed ridge axis is also limited on its western margin by the extended Sayma shear zone here marked by some mica-bearing granitic intrusions (Rabu et al., 1986). Two of our studied samples 90OA62 (concordant stratiform) and 83OG58 (discordant dike), originate from Maqsad (Tuf area, Fig. 2a). These are end-members of multiple structural relationships illustrating the progressive transposition of chromite ores in the high-T flow structures of the enclosing peridotite (Fig. 12). The concordant pod emplaced atop the MTZ in flowing mantle. The discordant pod, not transposed, results from a last intrusion in the frozen lithosphere (Ceuleneer and Nicolas, 1985; Nicolas, 1989; Leblanc and Ceuleneer, 1992). This multiple association suggests that punctual melt feeders were concentrated in the given areas of Maqsad diapir, each active over a short time during a dynamic process which led the cooling mantle from spreading ridge condition, T~1200°C (Nicolas et al., 2000), to brittle lithospheric condition (Leblanc and Ceuleneer, 1992).

5. 3. Origin and significance of mantle-hosted chromitites

Melts capable of forming podiform chromite requires the involvement of water in the zone of melt generation. Water acts in promoting partial melting in depleted mantle, it also dissolves into the resulting melt (Edwards et al., 2000). Subduction of sub-oceanic mantle is the commonly invoked origin of water.

Accounting for the relationships of chromite ores with large mantle shear zones, could shear zones be a potential alternative hydration source? Marked by gabbro dike intrusions partially involved in the shear stem (Boudier et al., 1988), mantle shear zones are location of hydrous fluid circulation at depth. Being major elements in structuration of the northern ophiolite, they are part of the ridge tectonics and root in the asthenospheric oceanic mantle. However, trending sub-parallel to the spreading-ridge,

they are not transform. We infer that they may represent the conversion from spreading ridge to strike-slip tectonics (Atwater, 1989) at a ridge-trench margin of the type America-Pacific (Nicolas and Boudier, 2017).

The new interesting question points to the occurrence of UHP phases in chromites of some investigated ophiolites (Zhou et al., 1996; Xiong et al., 2003). These phases including zircon, titanite, corundum, kyanite, coesite, metal alloy, diamond and moissanite are of continental affinity and are dated as old as Proterozoic (Savelieva et al., 2007; Robinson et al., 2015). One of the UHP phase, moissanite (SiC) has been identified in the Shamis II site and in an Emirati site of Hayl. Like other moissanite occurrences, the Semail examples have a ^{12}C deficit incompatible with normal terrestrial reservoir (Trumble et al., 2009), and have thus been assigned to Proterozoic continental accretion. The present study documents the fact that chromite, crystallizing in situ in its exposure, would not encapsulate UHP phases at depth as proposed in various models (ie. Yang et al., 2015). Alternatively, in the Oman case, moissanite crystals would be trapped by melt ascending through the continental Arabian margin, and included in situ in the growing chromite crystals. The chromite tribute complements other records of possible continental contamination of the Semail ophiolite, adding credit to a complex model of ridge-trench collision at the origin of the exhumation of the Semail ophiolite (Gregory et al., 1998; Gray et al., 2005; Nicolas and Boudier, 2017; Boudier and Nicolas, 2018).

6. Conclusions

This study presents direct microstructural evidence for the in-situ crystallization of chromite ores in the Semail ophiolite. Olivine CPOs are similar in olivine-rich layers and in septa from chromite layers marking a common deformation of the olivine aggregate solid framework by dislocation creep at high temperature and synchronous of the crystallization of chromite. Chromite grains replacing olivine crystalized from a melt circulating in an open system, within a stress-bearing network of dunitic aggregate, whose deformation is controlled by olivine high-T slip system. The ratio of random boundaries favoring melt percolation, to twin boundaries enhancing the resistance to olivine corrosion, suggests that chromitite layers may represent planes of channelized fluid circulation.

Chromite crystallized in ductile mantle flowing, in the vicinity of an active spreading ridge under asthenospheric conditions, but also controlled by lithospheric shear zones that may relate to ophiolite exhumation stage. Shear zones are acting as potential sources of hydration. A ridge-trench margin stem is a candidate accounting for the complexity of the ridge tectonics observed, the dual geochemical signatures, the eventual thermal conditions capable to generate Cr-bearing melt.

Our results have consequence on the relationships of chromite crystals with potential UHP phases. These phases of continental affinity have not been encapsulated at depth of origin, but possibly transported by Cr-bearing melts ascending through the Arabian margin, meeting with other evidences of continental contamination recorded in the Semail ophiolite.

ACKNOWLEDGEMENTS

The field data referred in this paper account for the many years of collaboration with the Directorate of Minerals, Ministry of Commerce and Industry of the Sultanate of Oman. The first author thanks R.T. Gregory and R.G. Coleman for recent discussions on the Coast Range ophiolites of California. Andrea Tommasi provided manuscript clarifications. Reviews by Qin Wang and an anonymous reviewer are warmly acknowledged. C. Nevado and D. Delmas supplied high quality polished sections for EBSD measurements. The EBSD-SEM national facility in Montpellier is supported by the Institut National des Sciences de l'Univers (INSU).

REFERENCES

Ahmed, A.H., Arai, S., 2002. Unexpectedly high-PGE from the deeper mantle section of the northern Oman ophiolite and its tectonic implications. Contrib. Mineral. Petrol. 143, 263-278.

Arai, S., 1994. Characterization of spinel peridotites by olivine-spinel compositional relationships: Review and interpretation. Chem. Geol. 113, 191-204.

Arai, S., Kadoshima, K., Morishita, T., 2006. Widespread arc-related melting in the mantle section of the northern Oman ophiolite as inferred from detrital chromian spinels. J. Geol. Soc. London 163, 869-979.

Atwater, T., 1989. Plate tectonic history of the northeast Pacific and western North America, in: Winterer, E.L., D.M Hussong, D.M., Decker, R.W. (Eds.), The Eastern Pacific Ocean and Hawaii. Geol. Soc. Amer. N, 21-72.

Augé, T., 1987. Chromite deposits in the northern Oman ophiolite: Mineralogical constraints. Mineralium Deposita 22, 1-10.

Augé, T., Roberts, S., 1982. Petrology and Geochemistry of some chromiferous bodies within the Oman ophiolite. Ofioliti 7, 133-154.

Bachmann, F., Hieslscher, R., Schaeben, H., 2010. Texture Analysis with MTEX: Free and Open Sources Software Toolbox. Solid State Phenomena 160, 63-68. (https://mtex-toolbox.github.iol/)

Boudier, F., Ceuleneer, G., Nicolas, A., 1988. Shear zones, thrusts and related magmatism in the Oman ophiolite: initiation of thrusting on an ocean ridge. Tectonophysics 151, 275-296.

Boudier, F., Nicolas, A., 1995. Nature of the Moho transition zone in the Oman ophiolite. J. Petrol. 36(3), 777-796.

Boudier, F., Al-Rajhi, A., 2014. Structural control on chromite deposits in ophiolites: the Oman case. Geol. Soc. London Spec. Publ. 392, 263-277.

Boudier, F., Nicolas, A., 2018. Synchronous seafloor spreading and subduction at the paleo-convergent margin of Semail and Arabia. Tectonics 37(9), 2961-2982. doi:10.1029/2018TC005099.

Cassard, D., Nicolas, A., Rabinowicz, M., Moutte, J., Leblanc, M., Prinshofer, A., 1981. Structural classification of chromite pods in Southern New-Caledonia. Econ. Geol. 76, 805-831.

Ceuleneer, G., Nicolas, A., 1985. Structures in podiform chromite from the Maqsad district (Sumail ophiolite, Oman). Mineral Deposita 20, 177-185.

Christiansen, F.G.,1985. Deformation fabrics and microstructures in ophiolitic chromitites and host ultramafics, Sultanate of Oman. Geol Rundschau 74, 61-76.

Edwards, S.J., Pearce, J., Freeman, J., 2000. New insights concerning the influence of water during the formation of podiform chromitite. Geol. Soc. Am. Spec. Pap. 349, 139-148.

Gray, D.R., Miller, J.M, Gregory, R.T., 2005. Strain state and kinematic evolution of a fold nappe beneath the Semail ophiolite, Oman. J. Struct Geol. 27(11), 1986-2007.

527 Gregory, R.T., Gray, D.R., Miller, J.M., 1998. Tectonics of the Arabian margin associated
528 with the formation and exhumation of high pressure rocks, Sultanate of Oman.
529 Tectonics 17(5), 657-670.
530 Higgie, K., Tommasi, A., 2012. Feedback between deformation and melt distribution in
531 the crust-mantle transition zone of the Oman ophiolite. Earth Planet. Sci. Lett. 359-
532 360, 61-72.
533 Jousselin, D., Nicolas A., Boudier, F., 1998. Detailed mapping of a mantle diapir below a
534 paleo spreading center in the Oman ophiolite. J Geophys Res. 103, 18153-18170.
535 Lago, B.L., Rabinowicz, M., Nicolas, A., 1982. Podiform chromite ore bodies: a genetic
536 model. J. Petrol. 23, 103-125.
537 Leblanc, M., Ceuleneer, G., 1992. Chromite crystallization in a multicellular magma flow:
538 Evidence from a chromitite dike in the Oman ophiolite. Lithos 27, 231-257.
539 Lorand, J.P., Ceuleneer G., 1989. Silicate and base-metal sulfide inclusions in chromites
540 from the Maqsad area (Oman ophiolite-Gulf of Oman): A model for entrapment.
541 Lithos 22, 173-190.
542 Mainprice, D., Bachmann, F., Hielscher, R., Schaeben, H., 2014. Descriptive tools for the
543 analysis of texture projects with large datasets using MTEX: strength, symmetry and
544 components, in: Faulkner, D.R., Mariani, E., Mecklenburgh, J. (Eds.), Rock
545 Deformation from Field, Experiments and Theory. Geol. Soc. London Spec. Publ. 409,
546 251-271. http://dx.doi.org/10.1144/SP409.8
547 Michel, J.C., 1993. Mineral occurrence and metallogenic map of the Sultanate of Oman, at
548 scale 1:1,000,000 with explanatory notes. Directory General of Minerals, Oman, pp
549 40.
550 Michibayashi, K., Ina, T., Kanagawa, K. 2006. The effect of dynamic recrystallization on
551 olivine fabric and seismic anisotropy: Insight from a ductile shear zone, Oman
552 ophiolite. Earth Planet. Sci. Lett 244, 695-708.
553 Nicolas, A., 1989. Structures of ophiolites and dynamics of oceanic lithosphere. Kluwer
554 academic publisher, Dordrecht, Netherland, 367 p.
555 Nicolas, A., Poirier, J.P., 1976. Crystalline plasticity and solid state flow in metamorphic
556 rocks. Wiley-Interscience, London, 444p.
557 Nicolas, A., Al-Azri, H., 1991. Chromite-rich and chromite-poor ophiolites: The Oman
558 case, in: Peters, T., Nicolas, A., Coleman R.G. (Eds.), Ophiolite Genesis and Evolution
559 of the Oceanic Lithosphere. Kluwer Academic Publishers, 261-274.

560 Nicolas, A., Boudier, F., Ildefonse, B., Ball, E., 2000. Accretion of Oman and United Arab
561 Emirates ophiolite: Discussion of a new structural map. Mar. Geophys. Res. 21,147-
562 179.
563 Nicolas, A., Boudier, F. 2017. Emplacement of Semail-Emirates ophiolite at ridge-trench
564 collision. Terra Nova 29(2), 127-134. doi: 10.1111/ter.12256.
565 Poirier, J.P., Nicolas, A., 1975. Deformation-induced recrystallisation by progressive
566 misorientation of subgrain-boundaries, with special reference to mantle peridotites.
567 J. Geology 83, 707-720.
568 Rabu, D., Bechennec, F., Beurrier, M., Hutin, G., 1986. Geological map of Nakhl. Ministry
569 Petroleum Minerals, Sultanate Oman, Sheet NF 40-3E.
570 Robinson, P.T., Bai, W.J., Malpas, J., Yang, J.S., Zhou, M.F., Fang, Q.S., Hu, X.F., Cameron, S.,
571 Staudigel, H., 2004. Ultra high pressure minerals in the Luobosa ophiolite, Tibet, and
572 their tectonic implications. Geol.. Soc. London Spec. Publ. 226, 247-271.
573 Robinson, P.T., Trumbull, R.B., Schmitt, A., Jing-Sui, Y., Erzinger, J., Dare, S., Xiong, F.,
574 2015. The origin and significance of crustal minerals in ophiolitic chromitites.
575 Gondwana Res. 27, 486-506.
576 Rollinson, H.R., 2008. The geochemistry of mantle chromitites from the northern part of
577 the Oman ophiolite: inferred parental melt compositions. Contr. Mineral. Petrol. 156,
578 273-288.
579 Rollinson, H.R., Adetunji, J., Youssif, A.A., Gismelseed, A.M., 2012. New Mössbauer
580 measurements of the $Fe^{3+}/\sum Fe$ in chromites from the mantle section of the Oman
581 ophiolite: evidence for the oxidation of the sub-oceanic mantle. Miner. Mag. 76, 579-
582 596.
583 Savelieva, G.N., Suslov, P.V., Larionov, A.N., 2007. Vendian tectono-magmatic events in
584 mantle ophiolitic complexes of the Polar Ural: U-Pb dating of zircon from chromitite.
585 Geotectonics41, 105-113.
586 Shimada, M., Kokawa, H., Wang, Z.J., Sato, Y.S., 2002. Optimization of grain boundary
587 character distribution for inter-granular corrosion resistant 304 stainless steel by
588 twin-induced grain boundary engineering. Acta Mater. 50, 2331-2341.
589 Trumbull, R.B., Yang, J.S., Robinson, P.T., Di Perro, S., Vennemenn, T., Weidenbeck, M.,
590 2009. The carbon isotope composition of natural SiC (moissanite) from the Earth's
591 mantle: new discoveries from ophiolites. Earth Planet. Sci. Lett. 146, 489-497.

592 Umino, S., Miyashita, S., Hotta, F., Adachi, Y., 2003. Along-strike variation of the sheeted
593 dike complex in the Oman Ophiolite: Insight into subaxial ridge segment structures
594 and the magma plumbing system. Geochem. Geophys. Geosyst. 4(9). doi:
595 10.1029/2001GC000233.
596 Xiong, F., Yang, J., Robinson, P.T., Dilek, Y., Milusi, I., Xu, X., Zhou, W., Zhang, Z., Rong, H.,
597 2017. Diamond discovered from high-Cr podiform chromites of Bulqiza, Eastern
598 Mirdita ophiolite, Albania. Acta Geol. Sinica 91, 801-840.
599 Yang, J.S., Meng, F.C., Chen, S.Y., Bai, W.J., Xu, X.Z., Zang, Z.M., Robinson, P.T., 2015.
600 Diamond, native elements and metal alloys from chromitite of the Ray-Iz ophiolite of
601 the Polar Urals. Gondwana Res. 27, 459-485.
602 Zhou, M.F., Robinson, P.T., Malpas, J., Li, Z., 1996. Podiform chromitites in the Luobusoa
603 ophiolite (Southern Tibet): Implication for Melt-Rock Interaction and Chromite
604 Segregation in the Uper Mantle. J. Petrol. 37, 5-21.
605

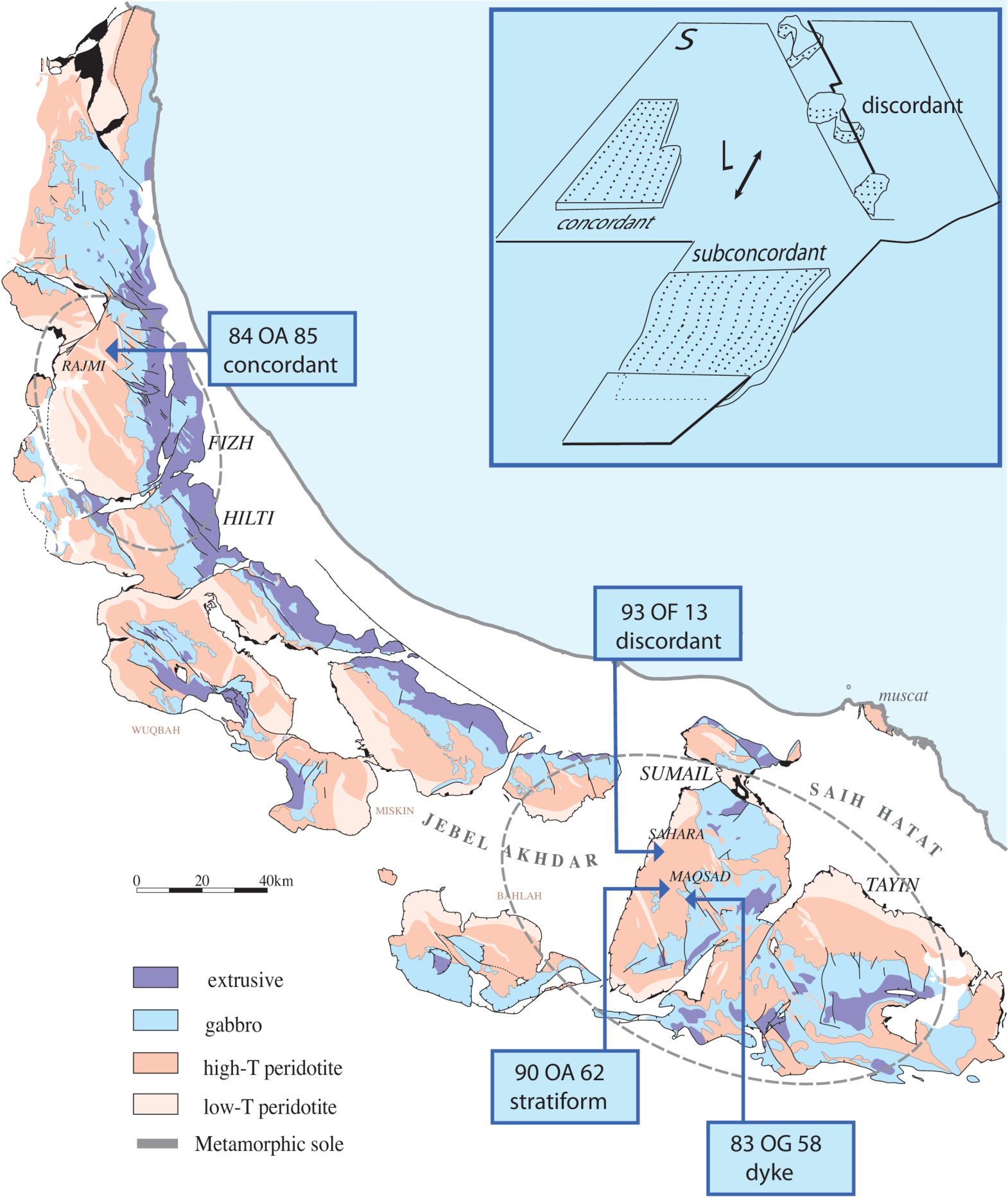

Figure 1. Location of studied sites of chromitite deposits on the structural map of Semail ophiolite (after Nicolas et al., 2000; Boudier & Al Raghi, 2014). High-T peridotite record asthenospheric solid state flow at T>1000°C. Low-T peridotite refer to shear zones developed in lithospheric conditions at 900°C<T<1000°C (Nicolas et al., 2000); dotted circles are chromite ore domains. Insert, structural classification of chromitite deposits after Cassard et al. (1981), S foliation, L lineation in enclosing peridotite.

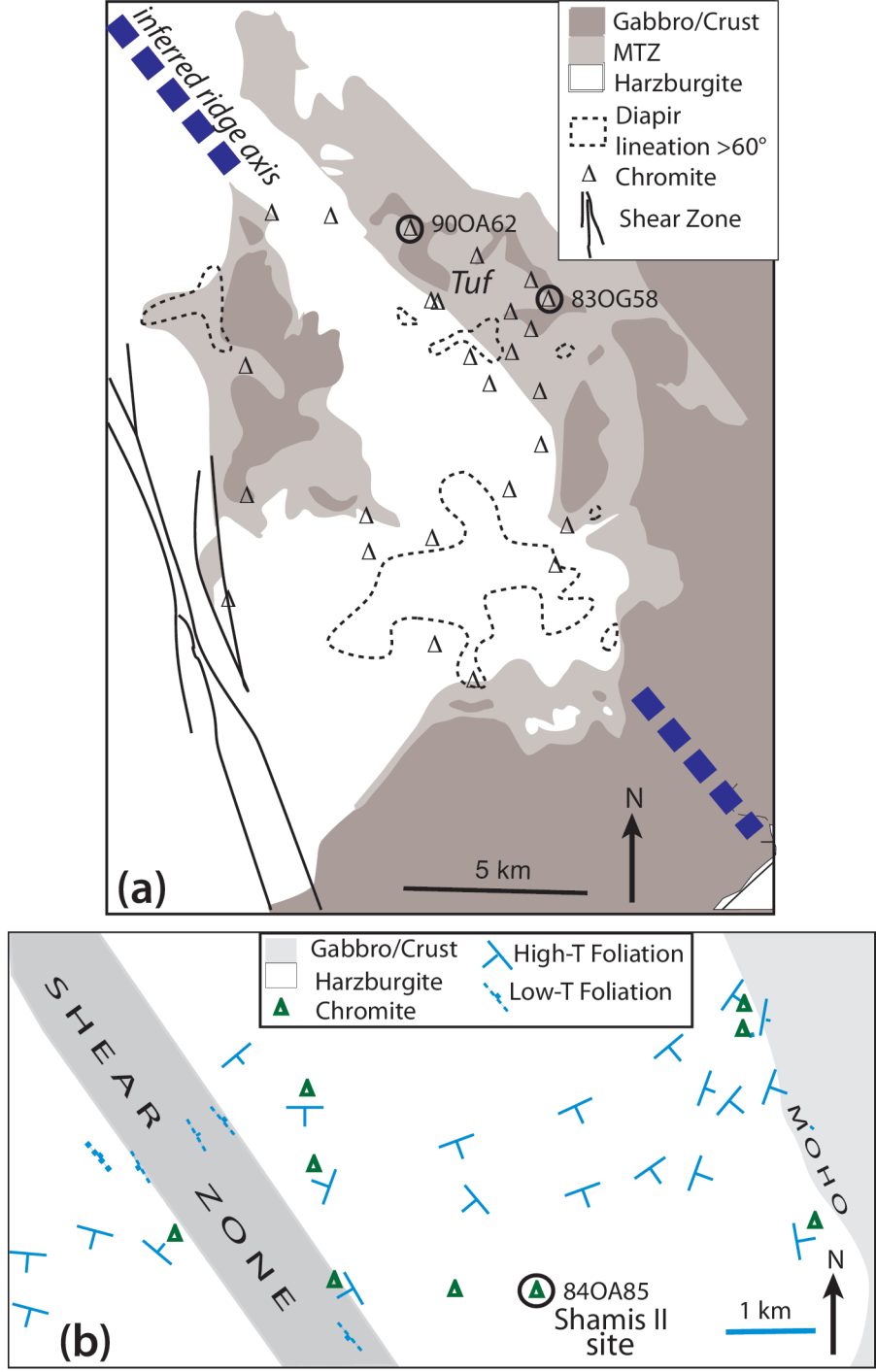

Figure 2. Localisation of samples studied in Maqsad site (a) and Wadi Rajmi site (b). Circled is studied ore.

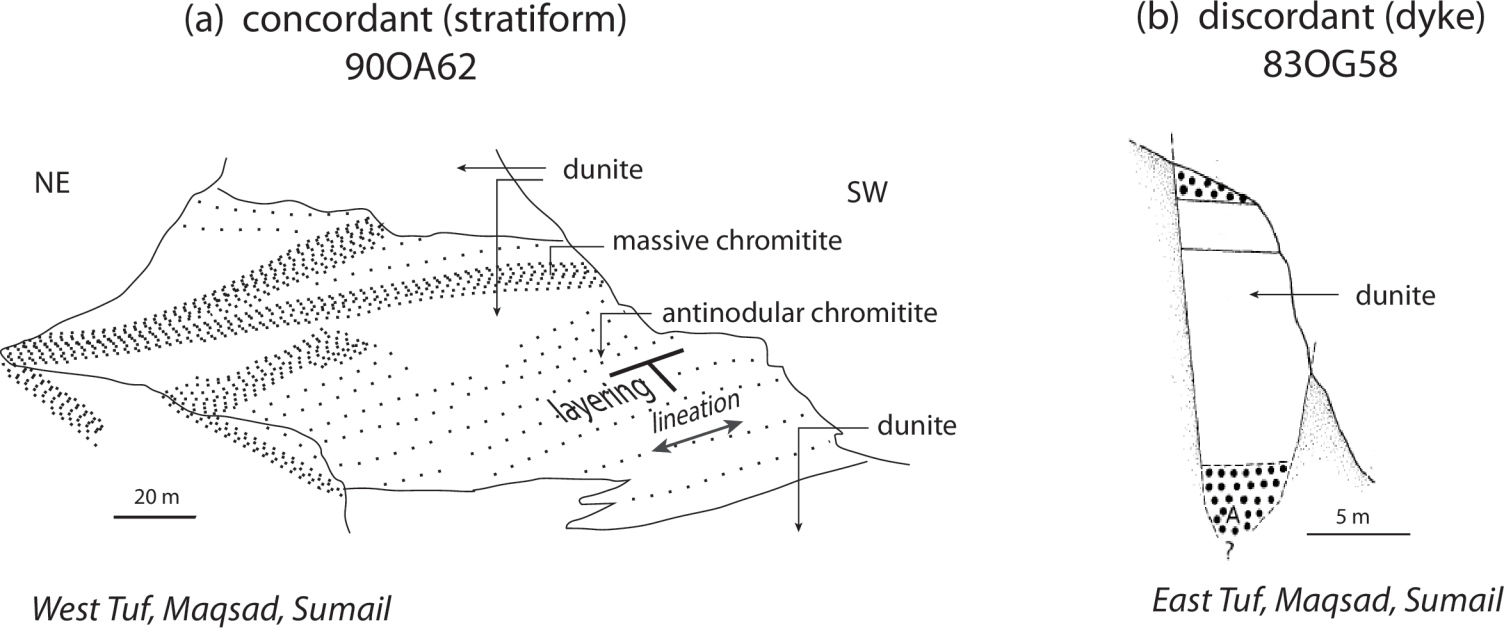

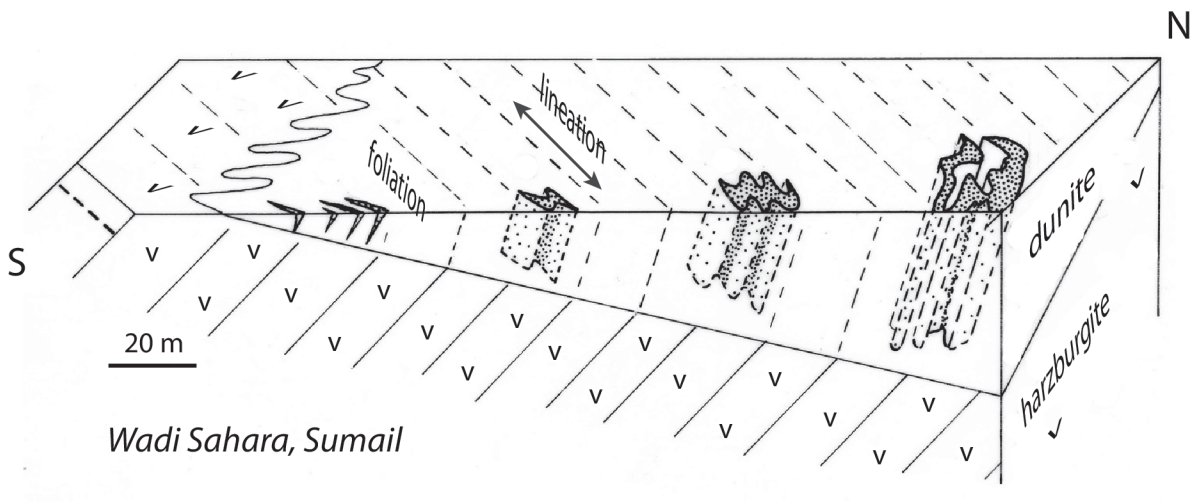

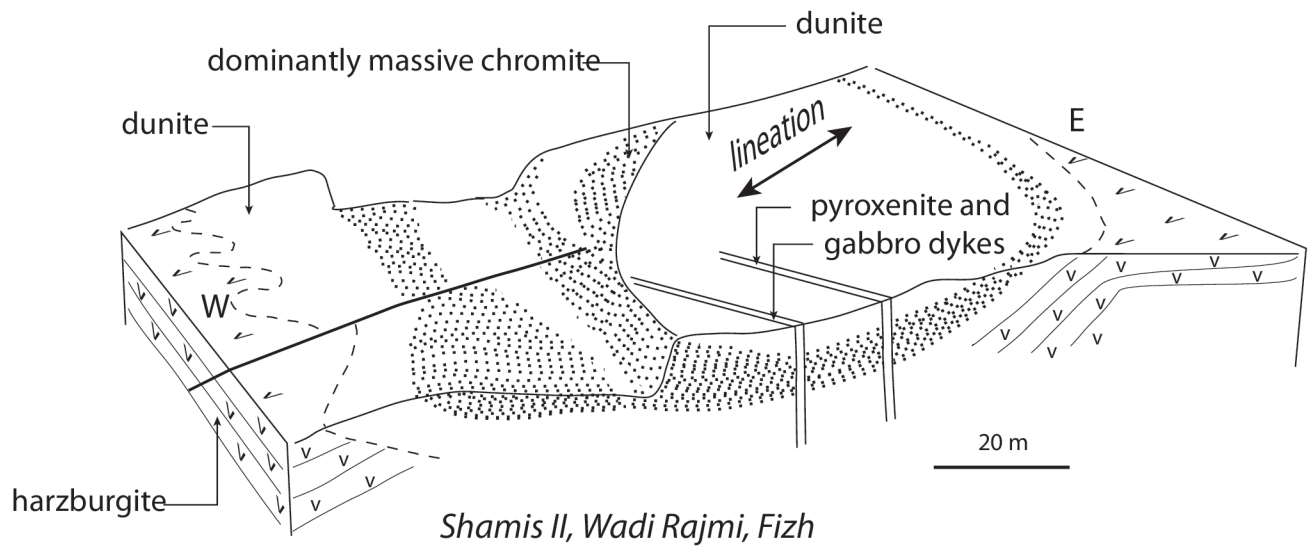

Figure 3. Structural sketch of studied chromitite deposits and their dunitic enclosure. Marked structures in the peridotite aggregate, foliation and lineation, indicated by spinel shape fabric on outcrop, are the record of asthenospheric mantle flow (Nicolas et al., 2000), flow plane and flow line respectively. Chromitite aggregate behaves as a passive marker.

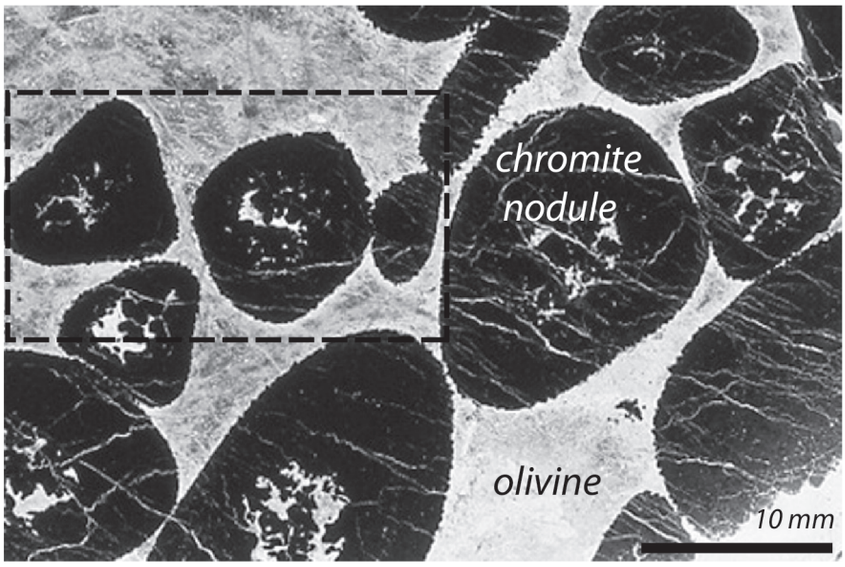

(a) nodular 83OG58

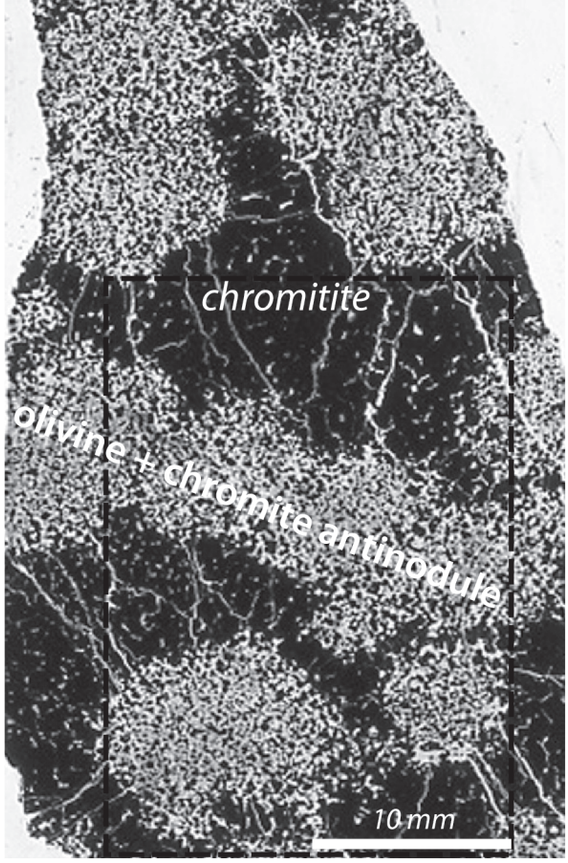

(c) antinodular 93OF13

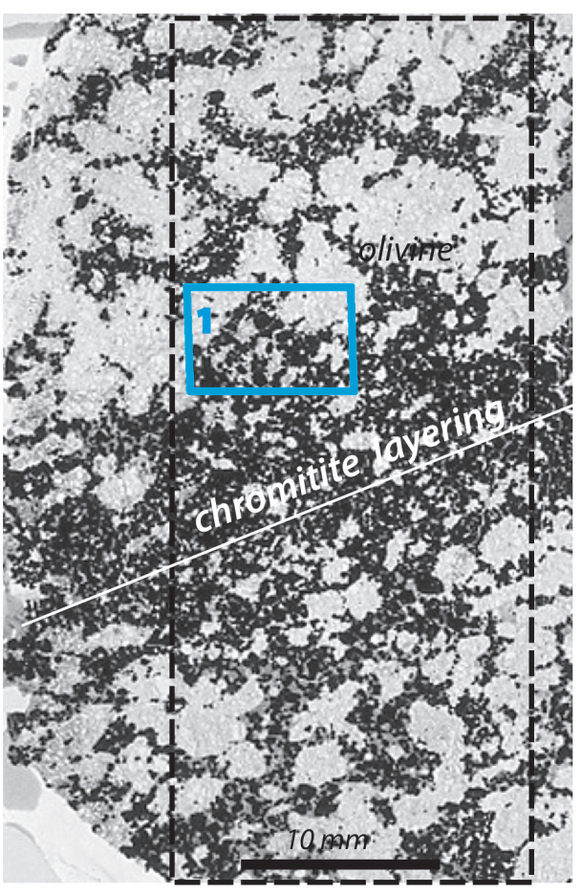

(b) interstitial 90OA62

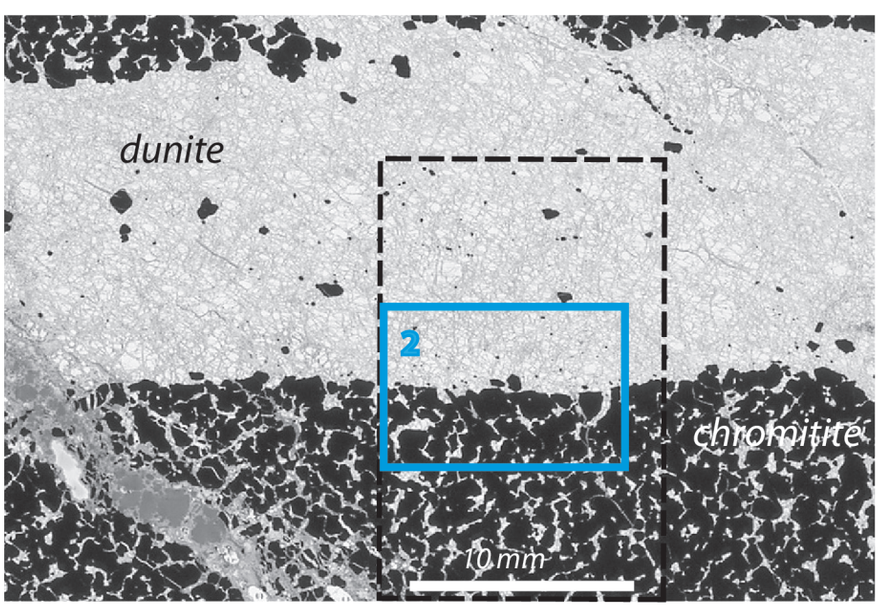

(d) massive 84OA85

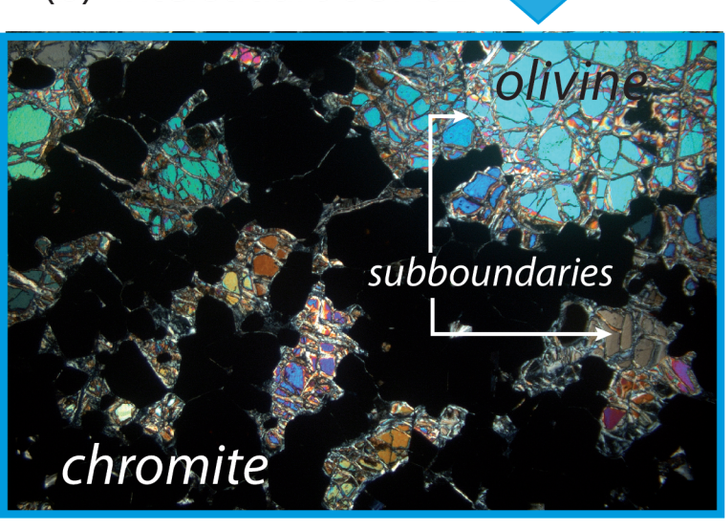

1

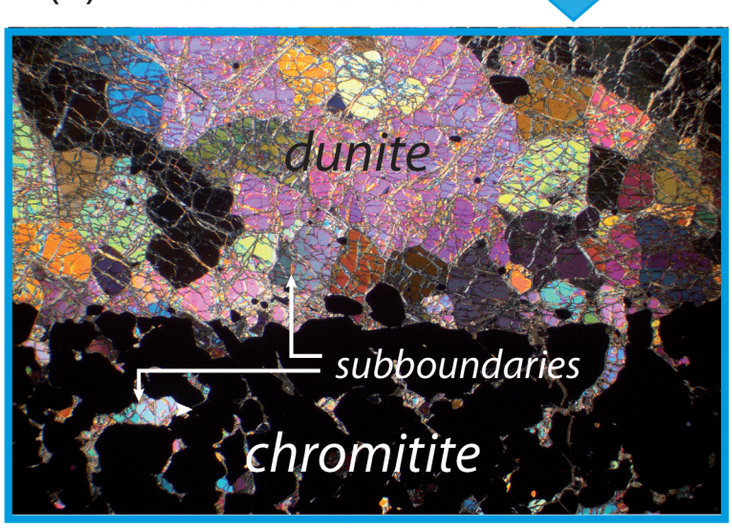

2

Figure 4. Chromitite textures in the four samples studied (optical microscope plane light). Thin sections are cut perpendicular to the chromite layering; textural types after Cassard et al. (1980). Doted insert, area explored by electron backscatter diffraction patterns (EBSD). Blue insert are zoom images (optical microscope plane polarized light): (1) detail of chromite/olivine grain boundaries concave toward olivine in interstitial texture; (2) contact of massive chromite including septa of interstitial olivine, with highly restored olivine in hosting dunite.

83 OG 58

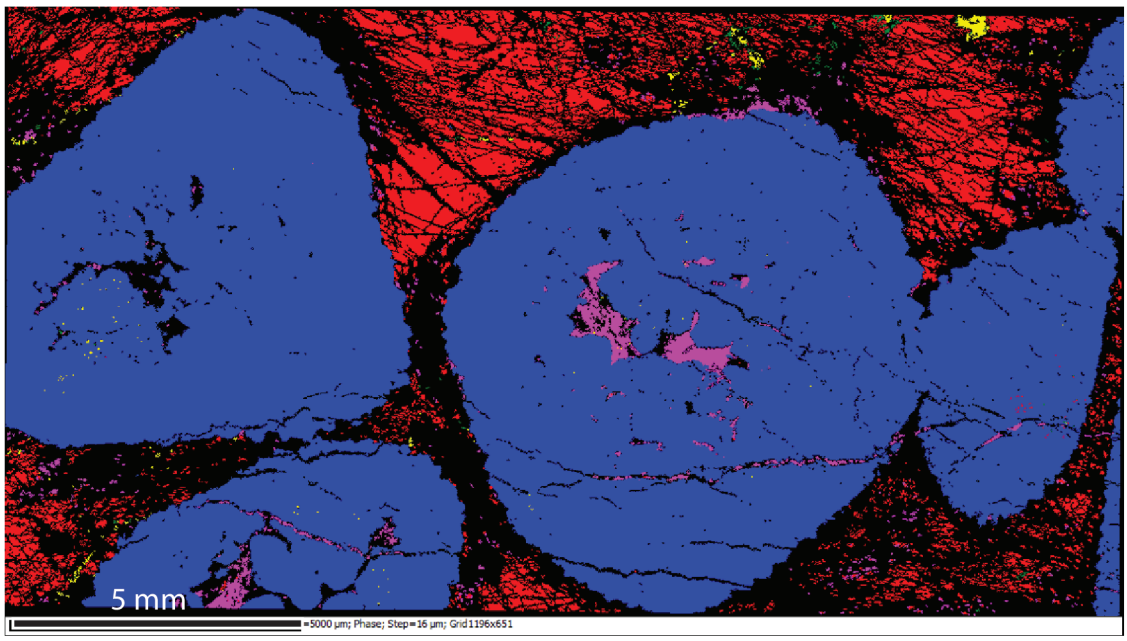

(a)

PHASE MAP

red, olivine
blue, chromite
pink, pargasite
yellow, chlorite
black, lizardite

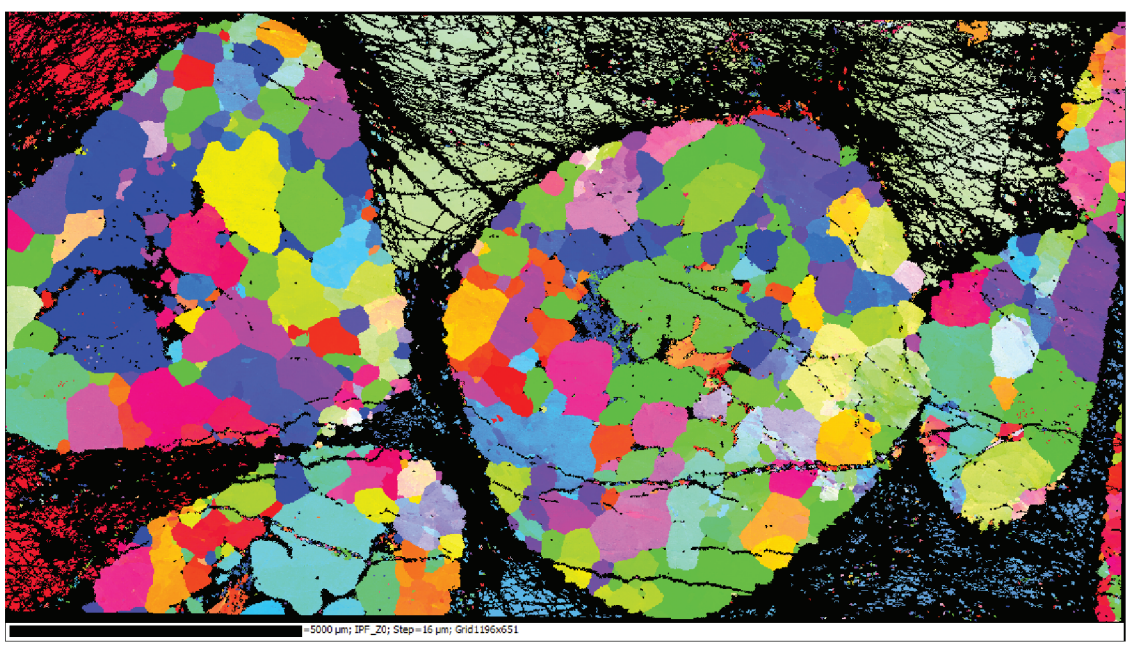

(b)

OLIVINE
& CHROMITE
orientation map

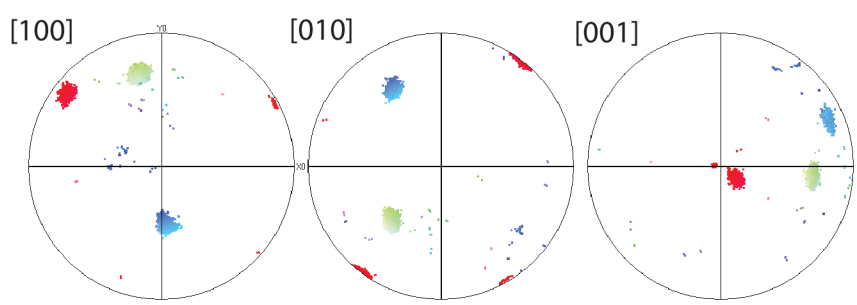

OLIVINE pole figure

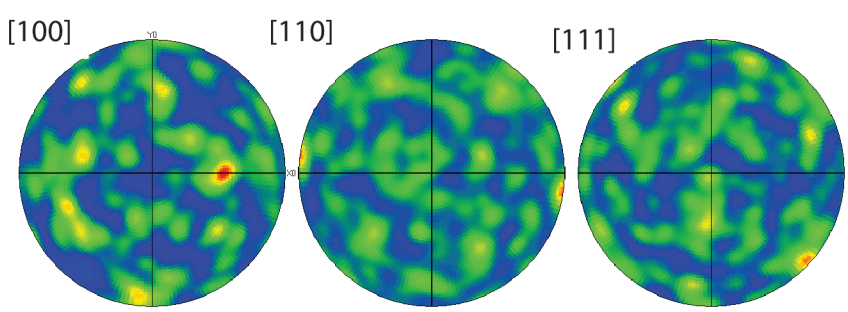

CHROMITE pole figure

min= 0.10
max= 4.61

(c)

Figure 5. Sample 83OG58, nodular type. EBSD pattern (studied area marked on figure 4a). a) phase map: b) orientation map of olivine and chromite. c) olivine and chromite pole figures. Thin section reference plane, lower hemisphere projection.

90 OA 62

(a) olivine orientation map & pole figure

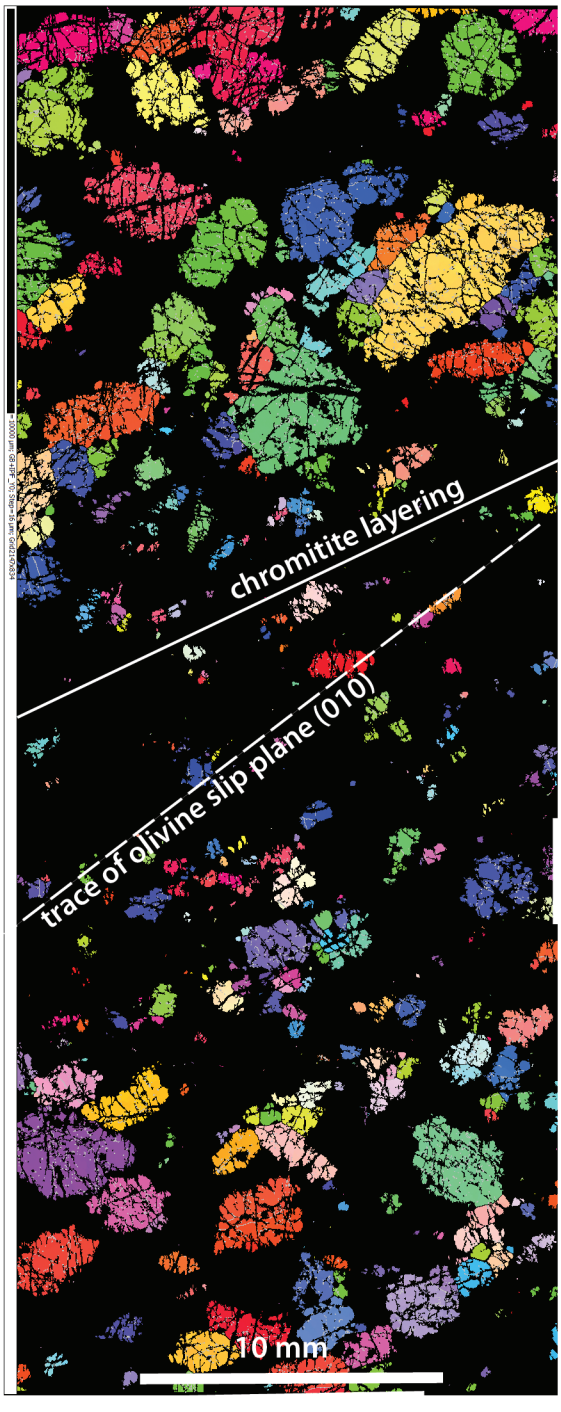

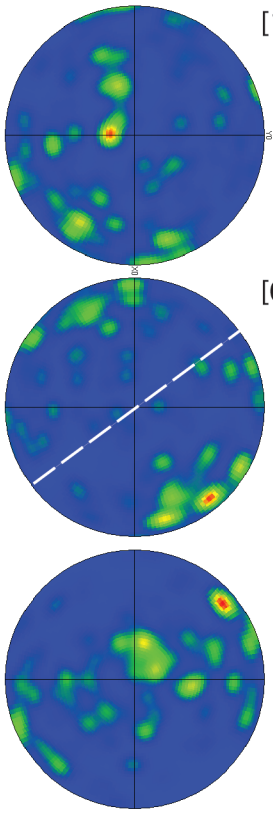

min= 0.0
max= 13.39

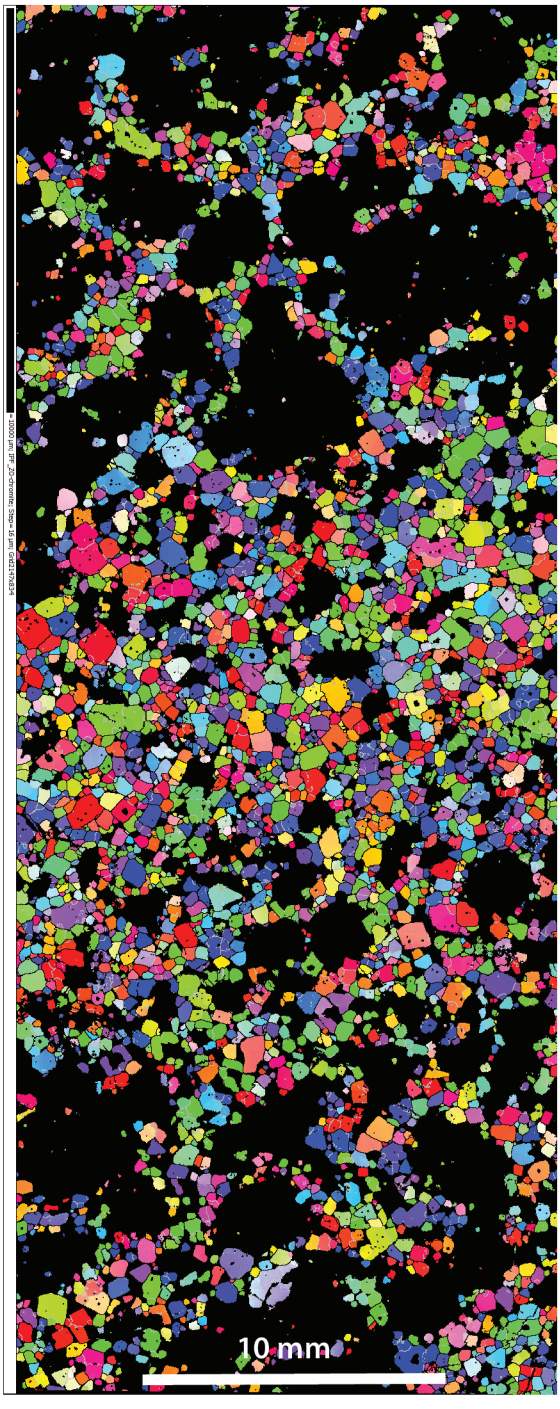

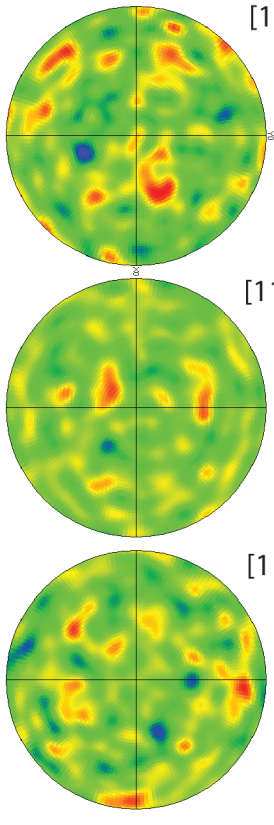

min= 0.55
max= 1.48

(b) chromite orientation map & pole figure

Figure 6. Sample 90OA62, interstitial type. EBSD exploration pattern of chromite rich layer with its olivine-rich surrounding (studied area marked on figure 4b). (a) Olivine orientation map and pole figure. Trace of olivine slip plane (010) is orthogonal to [010] point maximum in pole figure. (b) Chromite orientation map and pole figure. Pole figures cover the total area indexed in the orientation maps. Plane of projection is the thin section plane, not including XZ strain axes. Lower hemisphere of projection.

(a) olivine orientation map & pole figure

(b) chromite orientation map & pole figure

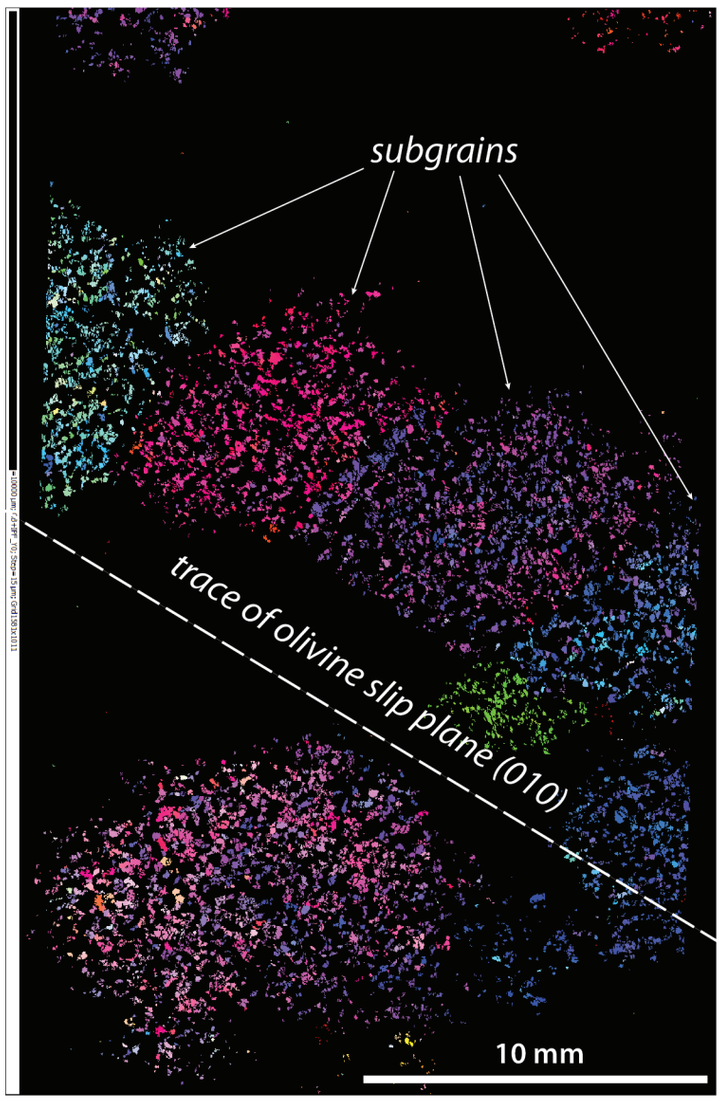

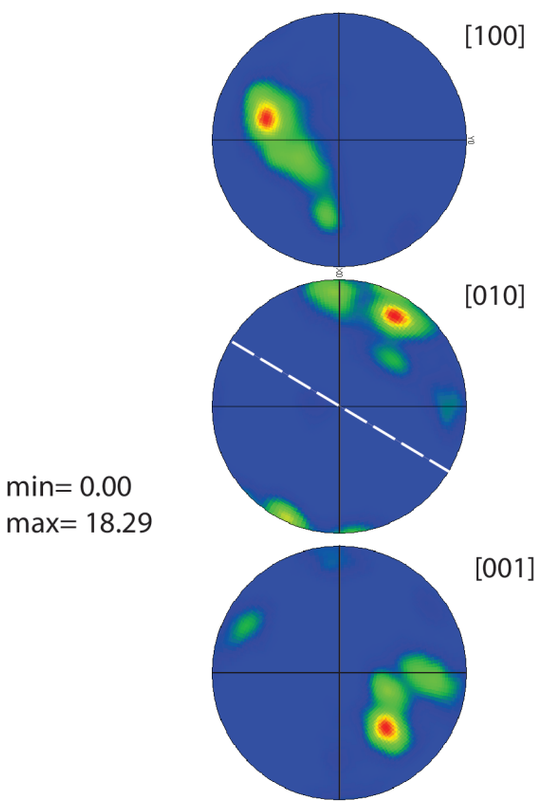

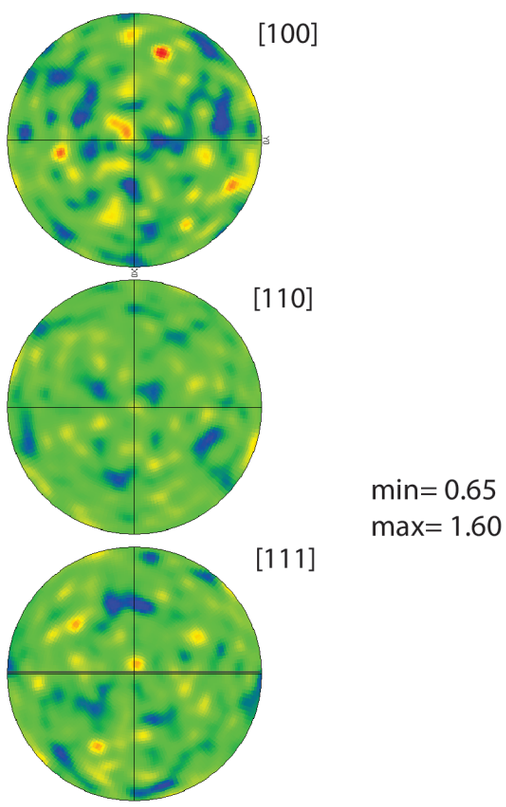

Figure 7. Sample 93OF13, antinodular type. EBSD pattern of mix olivine-chromite nodule within enclosing chromitite matrix (studied area marked on figure 4c). (a) Olivine orientation map and pole figure. Colour changes in elongated olivine nodule mark misorientation of subgrains. Trace of olivine slip plane (010) is orthogonal to [010] point maximum from olivine pole figure. (b) Chromite orientation map and pole figure. Pole figures cover the total area indexed in the orientation maps. Plane of projection is the thin section plane, not including XZ strain axes. Lower hemisphere of projection.

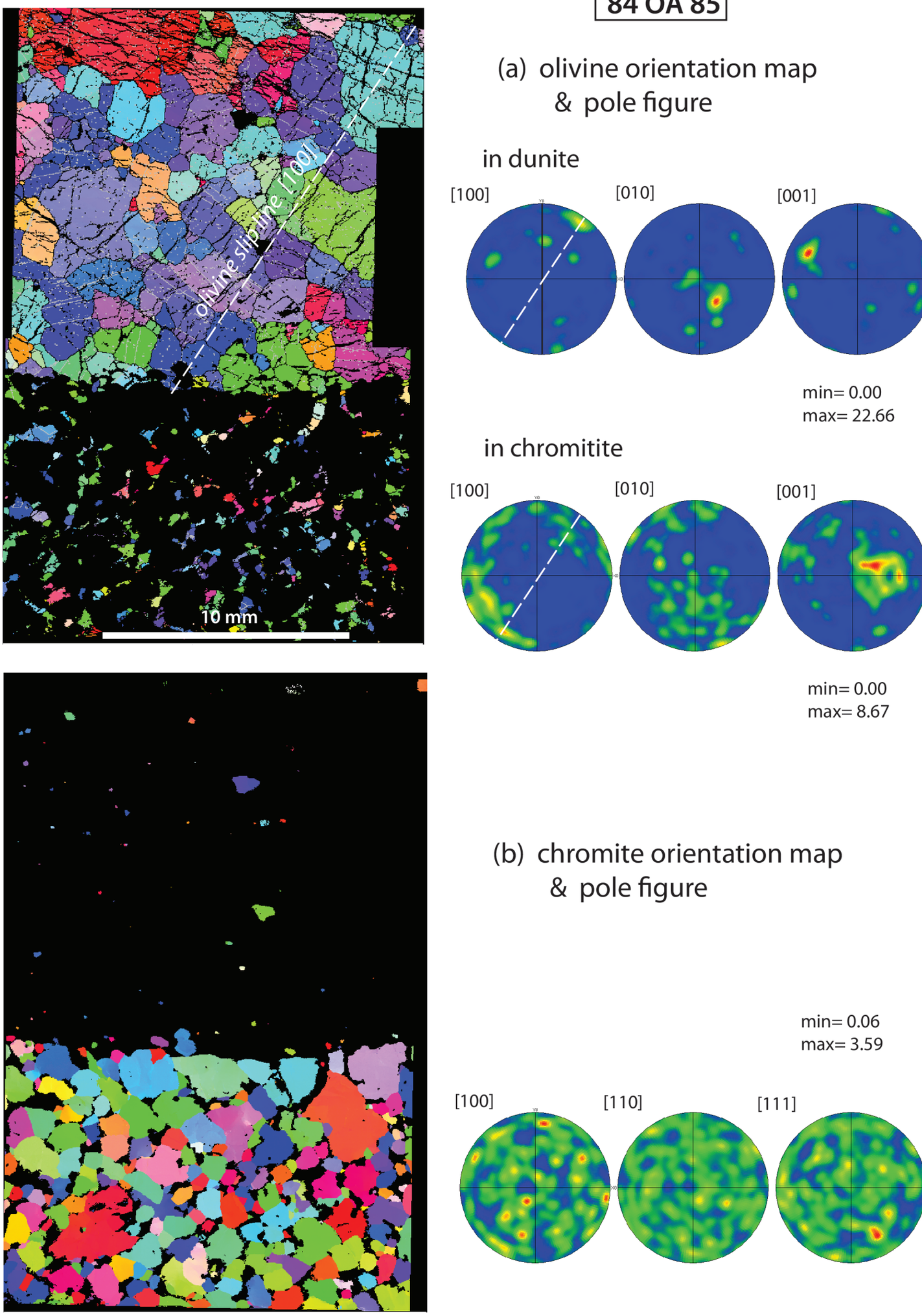

Figure 8. Sample 84OA85, massive chromitite. EBSD exploration pattern of massive chromitite band interlayered with dunite (studied area marked on figure 4d). (a) Olivine orientation map and pole figures measured separately in chromitite band and in enclosing dunite. Olivine slip line is traced parallel to [100] point maximum in dunite pole figure and perpendicular to straight (100) grain boundaries. (b) Chromite orientation map and pole figure in total area. Plane of projection is the thin section plane, cut perpendacular to layering, it happens to be close to parallel to the [100] slip line, but at high angle to the flow plane. Lower hemisphere of projection.

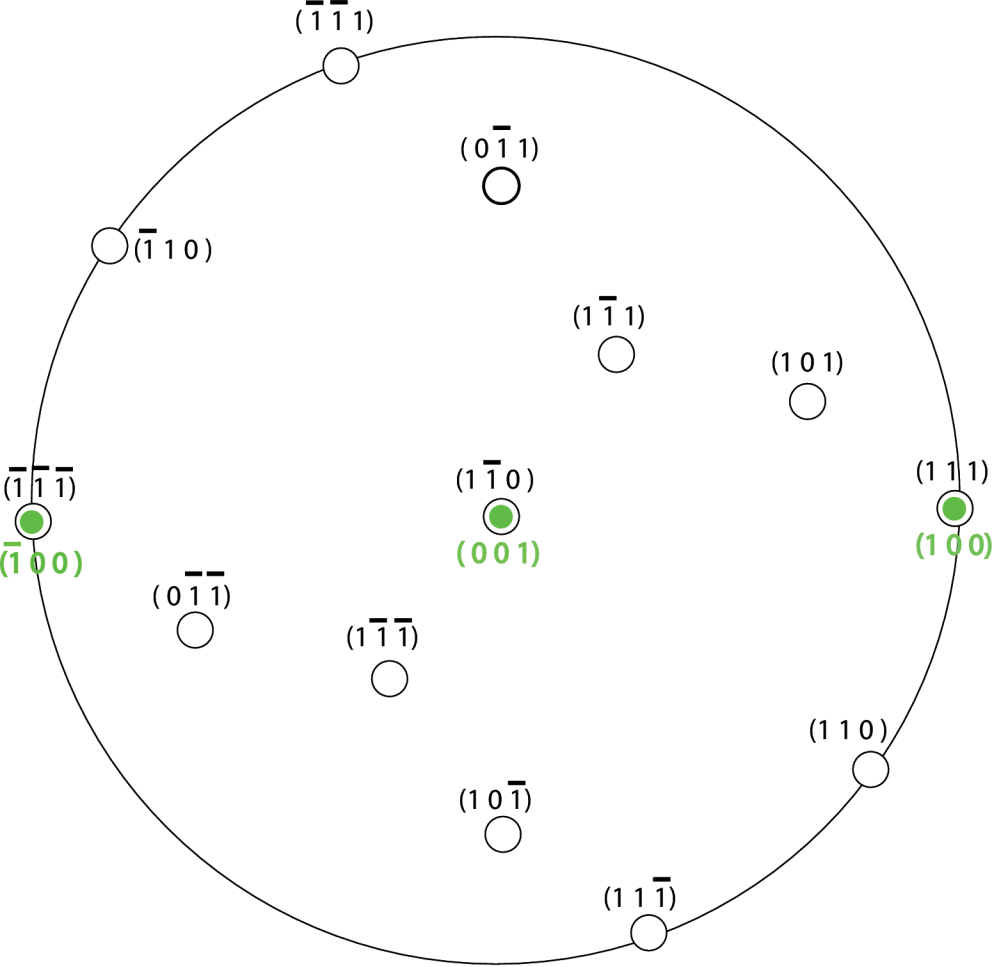

Figure 9. Topotactic relationships chromite (black), spinel structure with cubic crystal symmetry, to olivine (green), forsterite with orthorhombic crystal symetry. (111)Sp fit (100)Fo , and (110)Sp fit (001)Fo. Difference in d-spacing= 0.05.

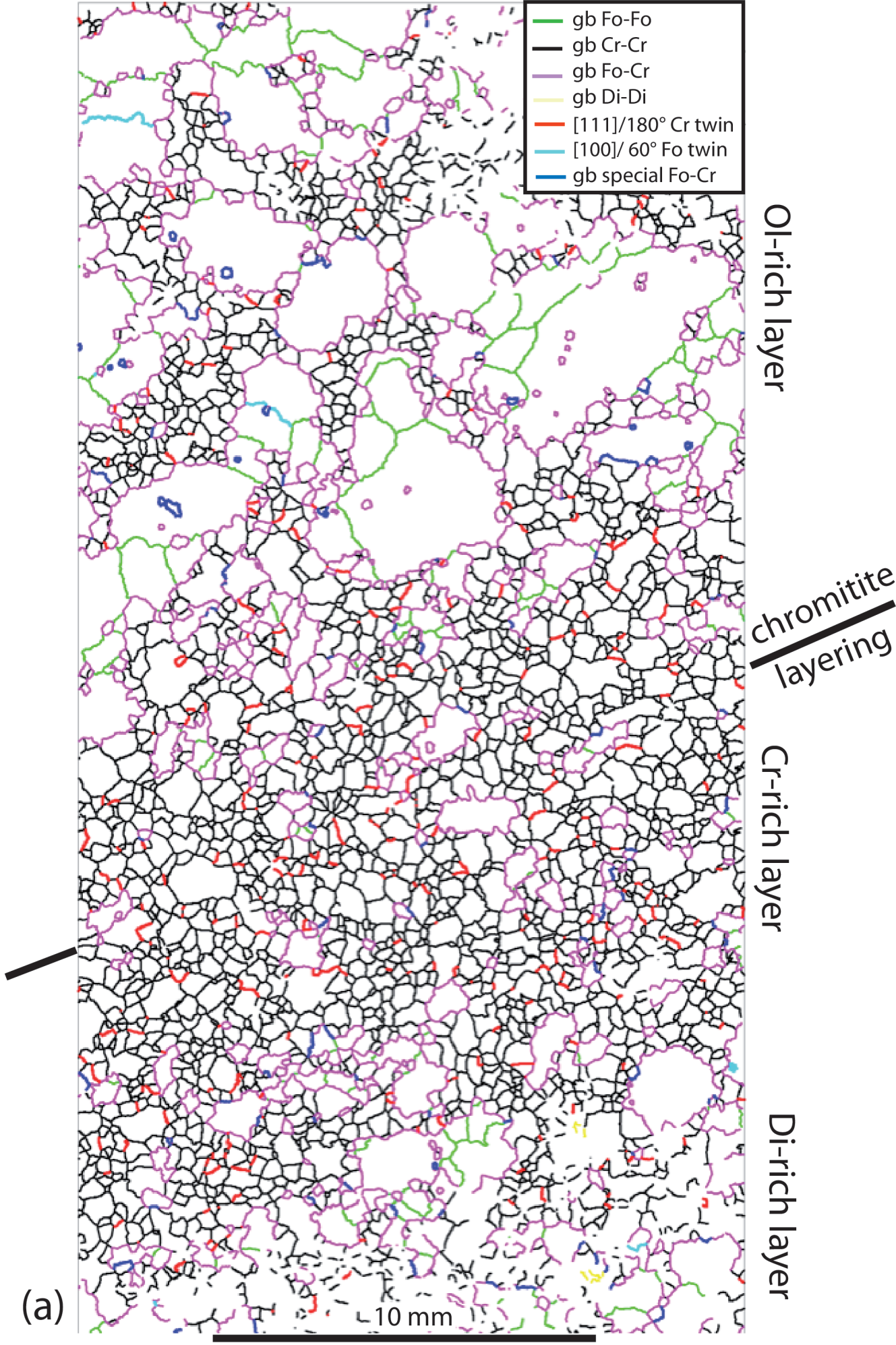

Figure 10 (a) MTEX large area mapping in thin section 90OA62 (see Fig. 6) with following boundaries detected: Fo-Fo random; Cr-Cr random; Fo-Cr random; Cr twin [111] /180°; Fo twin [100] /60°; Fo-Cr special (topotactic). Chromite-rich vs Olivine-rich bands are representative of chromite/dunite layering.

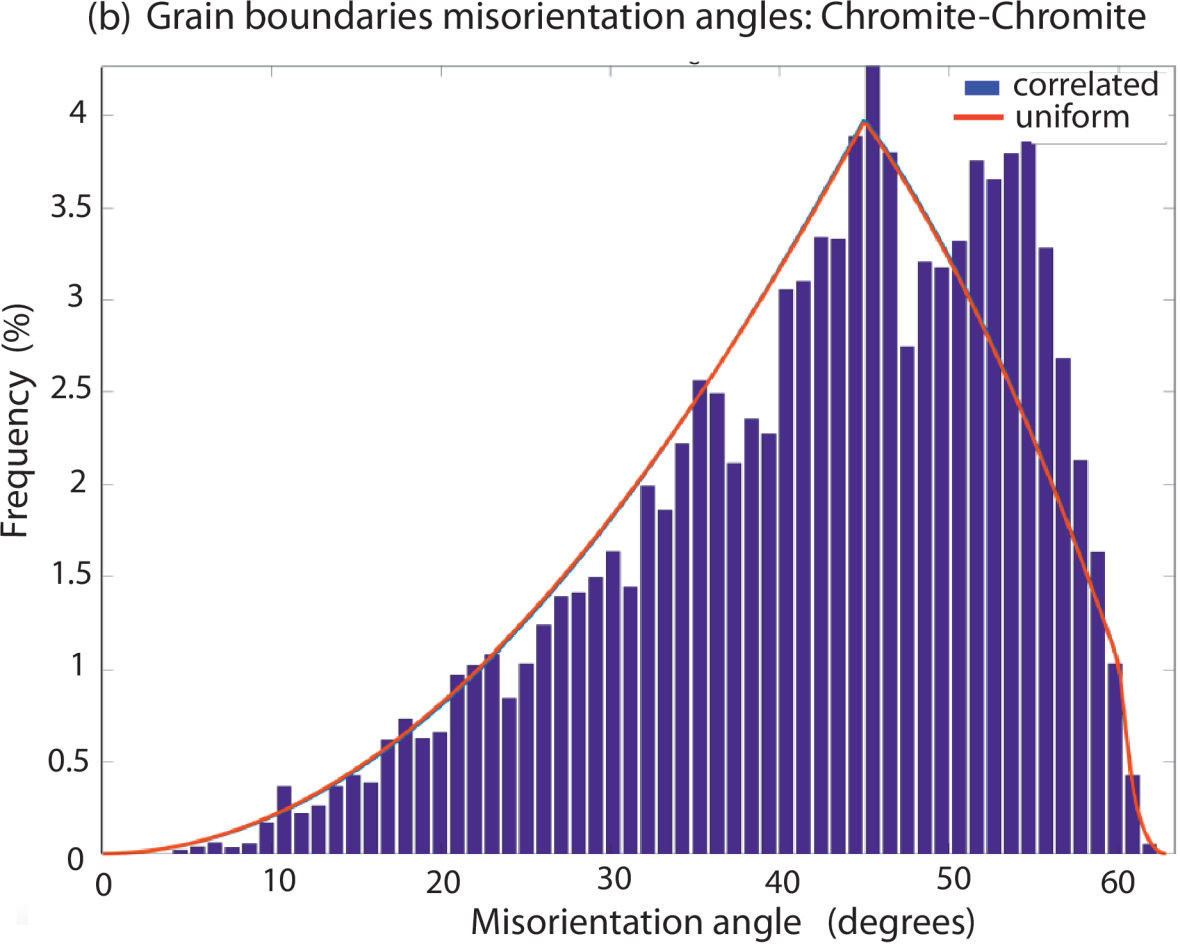

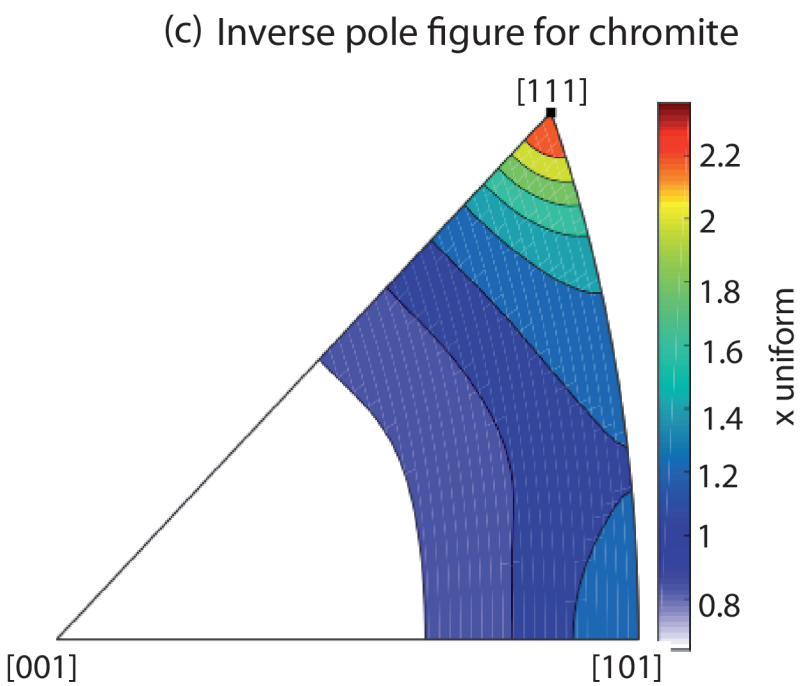

Figure 10 (b) Chromite-chromite misorientation angles distribution, that is close to theoretical uniform or random distribution (red line). (c) Inverse pole figure of grain rotation axis for chromite between [001], [111] and [101]. In contrast to the uniform misorientation angles, distribution of the misorientation axe indicates a maximum of 2.2 times uniform near [111], the chromite twin axis.

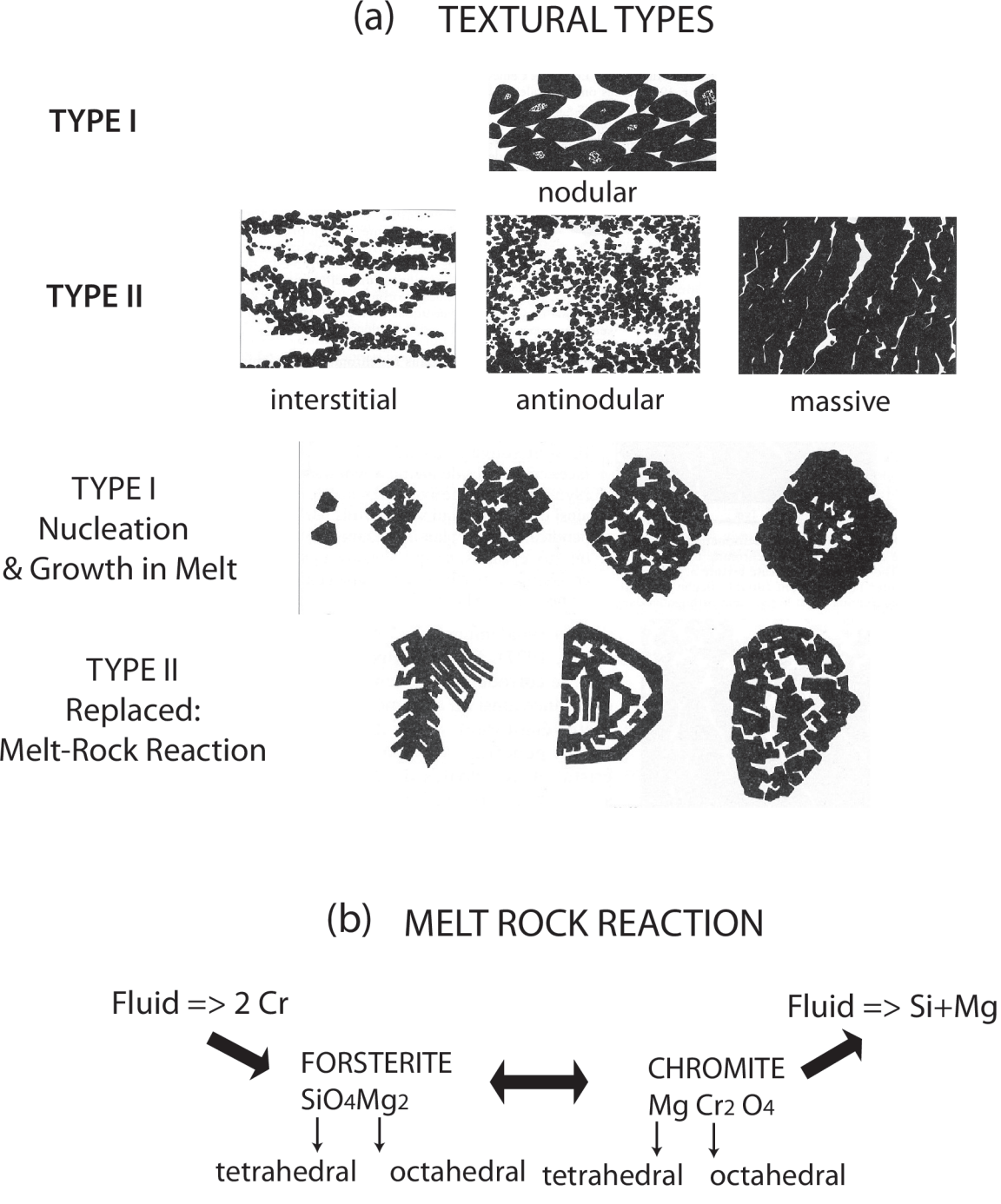

Figure 11. (a) Textural evolution. Type I, crystallization from a melt; Type II, melt-rock interaction. (b) Forsterite-Chromite phase transformation balance. Forsterite, hexagonal-close-packed arrangement with Si_{IV} and $(Mg,Fe)_{II}$ in tetrahedral and octahedral sites respectively; Chromite, cubic-close-packed arrangement with (Mg,Fe)II and (Cr,Al)III in tetrahedral and octahedral sites respectively. Forsterite unit cell=10, 6, 5 Å; Chromite unit cell ~8 Å.

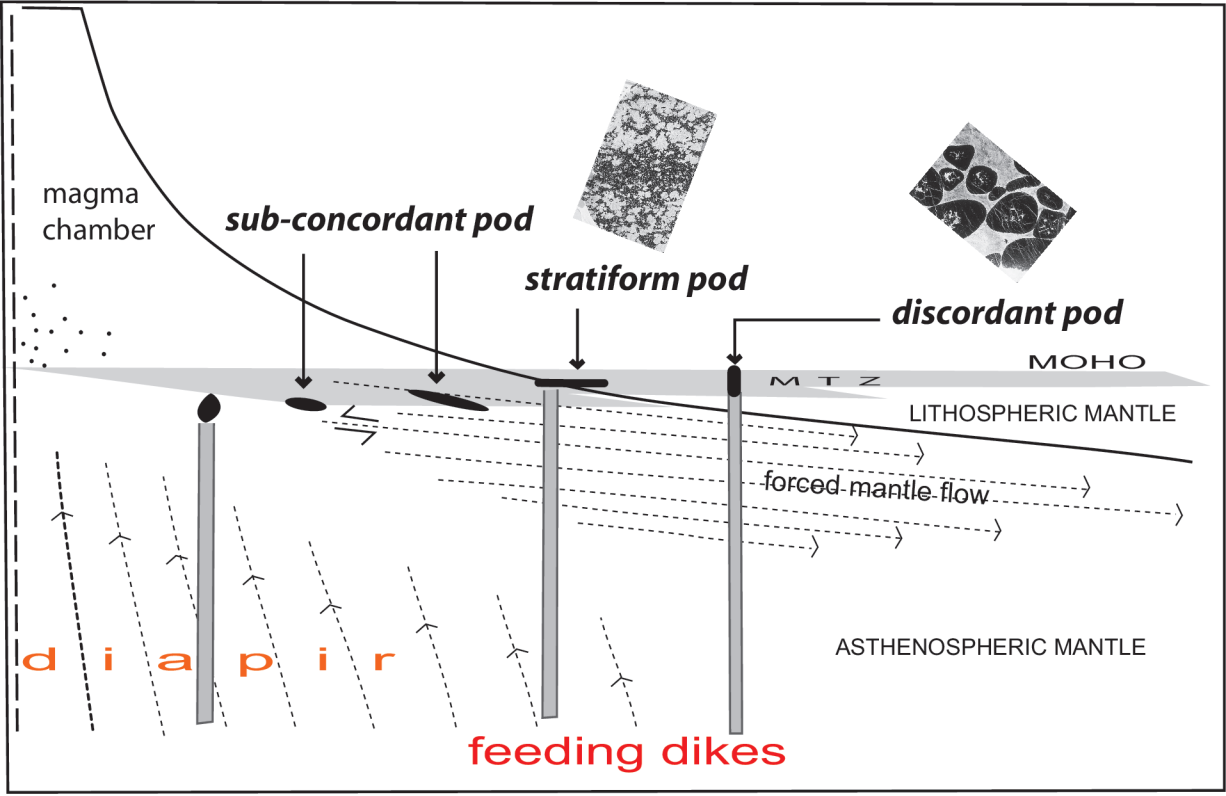

Figure 12. Conceptual evolution of ore deposits in Maqsad area. The sub-concordant pods corresponding to early injections at the base of the MTZ, are deformed and transposed in the asthenospheric mantle flow. The stratiform pod corresponds to injection in the MTZ, controlled by horizontal solid state flow in the cooling mantle. The discordant pod represents late melt injection in lithospheric conditions.